

Lepto-axiogenesis and the scale of supersymmetry

Patrick Barnes,¹ Raymond T. Co,² Keisuke Harigaya,³ and Aaron Pierce¹

¹*Leinweber Center for Theoretical Physics, Department of Physics,
University of Michigan, Ann Arbor, MI 48109, USA*

²*William I. Fine Theoretical Physics Institute, School of Physics and Astronomy,
University of Minnesota, Minneapolis, MN 55455, USA*

³*Theoretical Physics Department, CERN, Geneva, Switzerland*

(Dated: August 4, 2024)

Abstract

If the Peccei-Quinn field containing the QCD axion undergoes rotations in the early universe, the dimension-five operator responsible for neutrino masses can generate a lepton asymmetry that ultimately gives rise to the observed baryon asymmetry of the Universe. This lepto-axiogenesis scenario requires a flat potential for the radial direction of the Peccei-Quinn field, naturally realized in supersymmetric models. We carefully compute the efficiency of this mechanism for the Dine-Fischler-Srednicki-Zhitnitsky (DFSZ) and Kim-Shifman-Vainshtein-Zakharov (KSVZ) axion models and place lower bounds on the masses of scalar superpartners required to reproduce the observed baryon asymmetry. For the KSVZ model, we find an efficiency for generation of the asymmetry six times larger than the previously extant computation after including scattering channels involving superpartners. In this case, the superpartner scale should be above ~ 30 TeV for a domain wall number of one; the lower bound weakens for larger domain wall numbers. We find that the superpartner mass scale may also be as low as 30 TeV for the DFSZ model. In all cases, the lower bound on the superpartner masses is inversely proportional to the sum of the squares of the neutrino masses and so can strengthen as the upper bound on the neutrino mass improves. We identify the parameter space where the axion rotation can simultaneously produce axion dark matter via kinetic misalignment; in this case it is possible to put an upper bound of order PeV on the masses of scalar superpartners.

CONTENTS

1. Introduction	3
2. Dynamics of the rotating field	5
2.1. Initiation and evolution of rotation	6
2.2. Kinetic misalignment and production of axion dark matter	10
3. Computation of the baryon asymmetry	11
3.1. Basics of lepto-axiogenesis	11
3.2. KSVZ	15
3.3. DFSZ	16
4. Detailed analysis of the DFSZ model	17
4.1. Thermalization	17
4.2. No saxion domination	19
4.2.1. $n = 1$	19
4.2.2. $n = 2$	27
4.3. Saxion domination	29
4.3.1. $n = 1$	30
4.3.2. $n = 2$	32
4.4. Interpretation of results for one-field model	34
4.5. Q-balls	36
5. Discussion	39
Acknowledgements	41
A. Computation of chemical potentials	41
1. All interactions in equilibrium	41
2. Out of equilibrium Yukawa interactions	44
3. Out of equilibrium gaugino masses and μ -term	45
4. Results for C_i	47
B. Scaling of baryon asymmetry production	49
C. Constraints from supersymmetric relics	50
References	53

1. INTRODUCTION

The Peccei-Quinn (PQ) symmetry [1, 2] provides an attractive solution to the strong CP problem. The pseudo Nambu-Goldstone boson associated with this symmetry, the axion [3, 4], can have important implications for cosmology. It is a cold dark matter candidate, and it can also play a central role in the generation of the matter-antimatter asymmetry.

One possibility is that axion dark matter can be generated by the misalignment mechanism [5–7], wherein the axion field is displaced from the zero-temperature minimum of its potential in the early universe. In this case, the axion begins its motion from rest when the mass generated by the QCD anomaly becomes comparable to the Hubble expansion rate. However, similar to fields in models of Affleck-Dine baryogenesis, the complex PQ field that contains the axion may receive a kick at early times and rotate in field space. This has ramifications for cosmology. First, axion dark matter may be produced not from the misalignment mechanism, but rather the so-called “kinetic misalignment mechanism” [8, 9], wherein the energy contained in the motion in field space is converted to axions. The observed abundance of dark matter points to heavier, less weakly-coupled axions than in the conventional misalignment case. Second, there is a PQ charge associated with the angular momentum in field space. This is analogous to the baryon/lepton number carried by Affleck-Dine fields. In the presence of chirality- and baryon/lepton number-violating interactions, the PQ charge is converted to baryon number, a mechanism known as axiogenesis [10].

In its minimal form, axiogenesis does not simultaneously explain the dark matter and baryon abundances; once the dark matter abundance is fixed, too little baryon asymmetry is produced. A successful simultaneous prediction requires additional physics beyond the Standard Model [10–15] to increase the efficiency of the transfer of PQ charge to baryon number. A particularly simple solution takes advantage of lepton-number violation present when neutrino masses are explained by a Majorana mass, a scenario known as lepto-axiogenesis [16, 17]. The Majorana mass allows transfer of the PQ charge to baryon minus lepton number $B - L$, which can eventually be converted to baryon number by weak sphalerons.

In this paper, we revisit lepto-axiogenesis, considering both Dine-Fischler-Srednicki-Zhitnitsky (DFSZ) [18, 19] and Kim-Shifman-Vainshtein-Zakharov (KSVZ) [20, 21] axion models. We focus on the case where lepto-axiogenesis is embedded in a supersymmetric

model. As we will discuss below, supersymmetric scenarios provide the most natural setting for axiogenesis. As in the original lepto-axiogenesis proposal, lepton-number violation is provided by the supersymmetric generalization of the $\Delta L = 2$ Weinberg operator [22] that is responsible for neutrino masses, $(LH_u)(LH_u)$.

In the DFSZ case, the PQ field couples directly to the Higgs fields. Then, the non-trivial dynamics of the PQ field can impact the masses of the Higgs fields present in the Weinberg operator and therefore the transfer of the lepton asymmetry. On the other hand, in the KSVZ case the PQ field couples to heavy quarks and not directly to the fields of the Standard Model, so the above effect is absent.

The precise baryon asymmetry depends on the details of the cosmological history, including the reheat temperature T_R of the universe following inflation. In our discussion, we pay attention to constraints placed on T_R from, for example, avoiding disruption of Big Bang Nucleosynthesis (BBN) by superpartner decays [23, 24]. We also carefully account for whether various Yukawa interactions are in equilibrium throughout the thermal history. This can affect the efficiency of the asymmetry transfer.

In Sec. 2, we review the dynamics of the rotating field and how dark matter is produced in the kinetic misalignment mechanism. We then discuss the computation of the baryon asymmetry in Sec. 3. In comparison to Ref. [16], we take special care to account for the presence of superpartners, which impacts the rate at which the lepton asymmetry is generated. We then present detailed results for the DFSZ model including the thermalization of the PQ field in Sec. 4. The outcome of our analysis is a prediction for the minimum scale of supersymmetry-breaking scalar masses. We also find parameter space where dark matter and the baryon asymmetry may be simultaneously explained. The scalar superpartner masses are bounded from above ($\lesssim 300$ TeV), and the axion decay constant is predicted to be approximately 10^9 GeV. We also discuss the possible production of a non-topological soliton, which in principle could disrupt the prediction of the baryon asymmetry. In Sec. 5, we summarize the results. The scale of supersymmetry breaking required by this mechanism is consistent with that indicated by the observed Higgs boson mass.

2. DYNAMICS OF THE ROTATING FIELD

We define our complex PQ field P containing the axion as

$$P = \frac{(f_a N_{\text{DW}} + S)}{\sqrt{2}} e^{i\theta/N_{\text{DW}}}. \quad (2.1)$$

Here f_a is the decay constant, N_{DW} is the domain wall number, S is the radial direction which we call the saxion, and $\theta = a/f_a$ is the angular direction. We assume that the potential of S is nearly quadratic. This assumption allows large field values for S in the early universe. This is necessary for initiating the rotation in field space, as we will discuss below. A nearly quadratic potential can be naturally realized in supersymmetric theories, where the potential can be flat up to supersymmetry-breaking corrections. This is the case for a two-field model, with superpotential and soft masses given by

$$W = \lambda X(P\bar{P} - v_{\text{PQ}}^2), \quad V_{\text{soft}} = m_P^2 |P|^2 + m_{\bar{P}}^2 |\bar{P}|^2. \quad (2.2)$$

Here, X is a chiral multiplet whose F -term potential fixes the PQ-charged fields P and \bar{P} to $P\bar{P} = v_{\text{PQ}}^2$. Without loss of generality, we take $|P| \gg v_{\text{PQ}} \gg |\bar{P}|$ in the early universe. We may then consider effective single-field dynamics for P with a nearly quadratic potential $m_P^2 |P|^2$, while \bar{P} is fixed to a small field value by $\bar{P} = v_{\text{PQ}}^2/P$ and is irrelevant. X will be fixed near the origin because of the large mass $\simeq \lambda P$. A nearly quadratic potential is also achieved by a one-field model with logarithmic corrections [25]

$$V(P) = \frac{1}{2} m_S^2 |P|^2 \left(\ln \frac{2|P|^2}{f_a^2 N_{\text{DW}}^2} - 1 \right), \quad (2.3)$$

with m_S the mass of the saxion. The logarithmic corrections arise from the quantum corrections due to a Yukawa coupling of P , which can be that with the KSVZ quark in the KSVZ model, while extra fields are required in the DFSZ model.

In the one-field model, the mass of the fermionic superpartner of the axion, the axino, is generated by one-loop corrections and is suppressed relative to the typical scale of scalar soft masses. This tends to make the axino the lightest supersymmetric particle (LSP). In the two-field case, R - or supersymmetry-breaking effects will induce an axino mass of order the gravitino mass, and an axino LSP is less likely. If stable, an axino LSP has the

potential to be problematic because it will typically overclose the universe.¹ The axino may decay if R -parity violation is introduced, or an axino LSP could be avoided if a bino and/or Higgsino were sufficiently light. See Appendix C for details, where we also discuss potential constraints from BBN.

In both the one- and two-field models, assuming the simplest mediation scheme of supersymmetry breaking by Planck-suppressed interactions, the saxion mass is expected to be of the same order as the soft scalar masses of the Minimal Supersymmetric Standard Model (MSSM). We will see that this curvature impacts the rotation of the axion in field space and the generation of the baryon asymmetry, and so the scalar mass may be constrained or predicted. In the one-field model, the curvature of the potential depends logarithmically on the field value of S . When we present results, we neglect this logarithmic dependence. So, they apply directly to the two-field case, but a small correction should be applied when interpreting results in the context of the one-field model, see Sec. 4.4.

2.1. Initiation and evolution of rotation

During inflation, the presence of a Hubble-induced mass term can induce a large field value for P [26]. Then, at these early times, operators that explicitly break the PQ symmetry of the form

$$W = \frac{1}{q} \frac{P^q}{M^{q-3}} \quad (2.4)$$

can be enhanced, where q is an integer. Even if these operators are suppressed today so as to not spoil the solution to the strong CP problem, they can have important implications in the early universe.

The potential of P is, for $S \gg f_a$,

$$V(P) = (m_S^2 - c_H H^2) |P|^2 + \frac{|P|^{2q-2}}{M^{2q-6}} + \left(A \frac{P^q}{M^{q-3}} + \text{h.c.} \right), \quad (2.5)$$

where H is the Hubble expansion rate, A is a constant coming from R -symmetry breaking, and c_H , the coefficient of the Hubble-induced mass term, is a constant expected to be

¹ In general, we expect that the axino will thermalize via the supersymmetric analog of the couplings that thermalize the saxion (see Sec. 4.1), which would overproduce axinos. It is conceivable that saxion thermalization might not occur until temperatures near the EW scale, in which case supersymmetry-breaking masses would be non-negligible, and the axino might not thermalize even if the saxion does. However, we have checked that even in this case the suppressed freeze-in abundance of an axino LSP would be problematically large.

$\mathcal{O}(1)$ [26]. Here, m_S is a soft supersymmetry-breaking mass, which in the two-field case would be identified with m_P . We focus on gravity-mediated scenarios, where A is of the same order as m_S . The superpotential in Eq. (2.4) preserves a linear combination of PQ-symmetry and R -symmetry, so the explicit breaking of the $U(1)$ symmetry of P requires R -symmetry breaking. Assuming $c_H > 0$ and that the Hubble scale during inflation is larger than m_S , P is driven to a large field value where the Hubble-induced mass term and the $|P|^{2q-2}$ term balance with each other. After inflation, P follows the minimum where two terms balance with each other [26, 27]. When $3H \simeq m_S$, P begins oscillations. At the same time, the A -term provides a kick for P in the angular direction, and P begins to rotate. This occurs at a temperature T_{osc} ,

$$T_{\text{osc}} \simeq 4 \times 10^9 \text{ GeV} \left(\frac{m_S}{\text{TeV}} \right)^{\frac{1}{4}} \left(\frac{T_R}{10^9 \text{ GeV}} \right)^{\frac{1}{2}} \left(\frac{g_{\text{MSSM}}}{g_*(T_{\text{osc}})} \right)^{\frac{1}{8}} \quad \text{for } T_R < T_{\text{osc}}, \quad (2.6)$$

where T_R is the reheat temperature after inflation and g_* denotes the number of relativistic degrees of freedom in the bath with a full MSSM value of $g_{\text{MSSM}} = 228.75$. We assume that inflationary reheating proceeds via perturbative inflaton decay, and thus the scale factor R obeys $R^3 \propto T^{-8}$ during reheating [28]. The PQ charge density associated with the rotation is

$$n_\theta = \frac{i}{N_{\text{DW}}} \left(\dot{P}P^* - \dot{P}^*P \right) = -\dot{\theta} \left(f_a + \frac{S}{N_{\text{DW}}} \right)^2. \quad (2.7)$$

We normalize the charge density so that it coincides with $-\dot{\theta}f_a^2$ for $S = 0$. The charge density normalized by the entropy density for $T_R < T_{\text{osc}}$ can be computed as follows. The inflaton energy density ρ_{inf} scales in the same way as n_θ after the initiation of the rotation (as R^{-3}), so $n_\theta/\rho_{\text{inf}}$ remains constant until $T = T_R$. The result is

$$Y_\theta \equiv \frac{n_\theta}{s} = \frac{n_\theta}{\rho_{\text{inf}} \Big|_{T_{\text{osc}}}} \times \frac{\rho_{\text{inf}}}{s} \Big|_{T_R} \simeq 10 \left(\frac{3}{N_{\text{DW}}} \right) \left(\frac{A}{m_S} \right) \left(\frac{\text{TeV}}{m_S} \right) \left(\frac{T_R}{10^9 \text{ GeV}} \right) \left(\frac{S(T_{\text{osc}})}{10^{16} \text{ GeV}} \right)^2. \quad (2.8)$$

The A/m_S is the ratio of the potential gradient in the angular and radial directions at T_{osc} .

There is also energy density ρ_S stored in the oscillations of the radial mode S . Whether ρ_S is of importance depends on the cosmological history and at what temperature T_{th} this mode is thermalized. The saxion energy density may come to dominate the energy of the universe

if this thermalization is late. We comment on this scenario further at the end of this section. Following thermalization, the motion of the PQ field becomes circular due to PQ charge conservation: the radial mode dissipates, but much of the axial motion remains—for while part of the charge can be transferred into a charge asymmetry of particles in the thermal bath, it is free-energetically favored to keep almost all of the charge in the rotation [10, 29]. The field will rotate around the body of the potential, with the radial direction eventually settling down to its minimum $N_{\text{DW}}f_a$. The energy in rotation ρ_θ , accounting for both the potential and kinetic energy, is given as $-\dot{\theta}n_\theta$. Before the radial direction S reaches its minimum, which occurs at a temperature denoted by T_S , $\dot{\theta}$ is a constant, and conservation of the PQ charge implies the energy density of the rotation scales as matter, $\rho_\theta \propto R^{-3}$. For $T < T_S$, the scaling of the rotational energy density resembles that of kination, $\rho_\theta \propto R^{-6}$. This scaling can be derived by noting that conservation of charge $n_\theta R^3$ at constant radial field value implies $\dot{\theta} \propto R^{-3}$. When the saxion settles to its minimum at $T = T_S$, we know both $|\dot{\theta}| \simeq N_{\text{DW}}m_S$ and the PQ yield $Y_\theta = -\dot{\theta}f_a^2/s$, so we can derive

$$T_S \simeq 1.4 \times 10^6 \text{ GeV} \left(\frac{100}{Y_\theta} \right)^{\frac{1}{3}} \left(\frac{f_a}{10^9 \text{ GeV}} \right)^{\frac{2}{3}} \left(\frac{m_S}{10 \text{ TeV}} \right)^{\frac{1}{3}} \left(\frac{N_{\text{DW}}}{3} \right)^{\frac{1}{3}} \left(\frac{g_{\text{MSSM}}}{g_*(T_S)} \right)^{\frac{1}{3}}. \quad (2.9)$$

If the energy of the rotation dominates the energy of radiation at this time and if the saxion has already undergone thermalization (i.e. $T_{\text{th}} > T_S$), then this T_S is also the temperature T_{MK} at which the universe transitions from a matter-dominated to a kination-dominated one. This history is illustrated in Fig. 1. We denote the temperature at which the universe transitions from radiation domination to matter domination as T_{RM} . We emphasize that the matter domination we refer to here is domination by an energy density of rotation that scales as matter, not ordinary matter. This occurs at temperature

$$T_{\text{RM}} = \frac{4}{3}N_{\text{DW}}m_S Y_\theta = 4 \times 10^6 \text{ GeV} \left(\frac{Y_\theta}{100} \right) \left(\frac{m_S}{10 \text{ TeV}} \right) \left(\frac{N_{\text{DW}}}{3} \right). \quad (2.10)$$

This expression is general as long as no entropy is produced after T_{RM} , and Y_θ refers to the charge yield evaluated at T_{RM} . In particular, this result applies whether or not there was an era where the saxion came to dominate the energy density of the universe prior to T_{RM} .

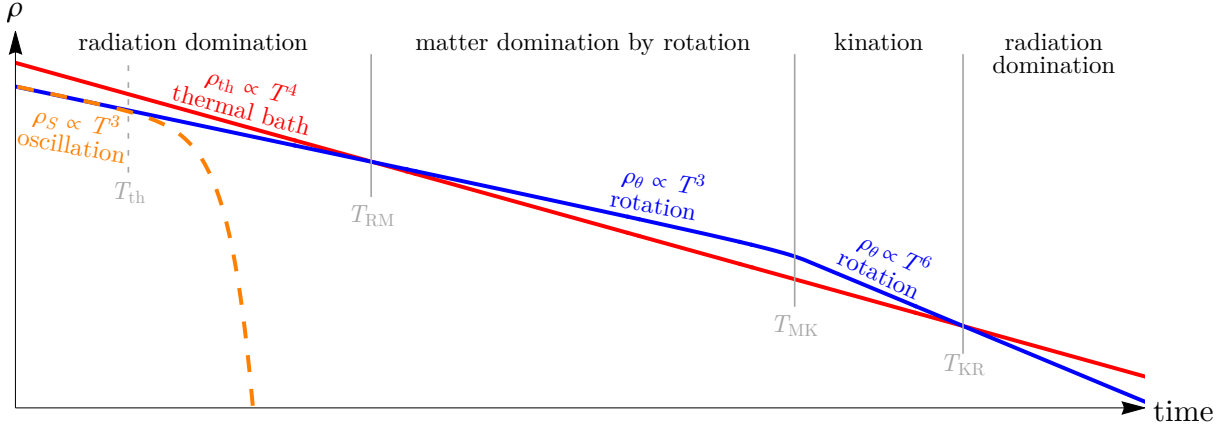


FIG. 1. An example evolution of energy densities as a function time for radiation (red), oscillations in the radial direction (orange), and rotations of the PQ-breaking field (blue). Relevant temperatures are labeled in gray and corresponding cosmological eras are labeled in black.

The kination-dominated era ends by the redshift of $\rho_\theta = \dot{\theta}^2 f_a^2 / 2 = n_\theta^2 / (2f_a^2)$ at temperature

$$T_{\text{KR}} = \left(\frac{135}{4\pi^2 g_*} \right)^{\frac{1}{2}} \frac{f_a}{Y_\theta} \simeq 1.2 \times 10^6 \text{ GeV} \left(\frac{100}{Y_\theta} \right) \left(\frac{f_a}{10^9 \text{ GeV}} \right) \left(\frac{g_{\text{MSSM}}}{g_*(T_{\text{KR}})} \right)^{\frac{1}{2}}. \quad (2.11)$$

A matter-dominated era followed by a kination-dominated one would modify the primordial gravitational wave spectrum in a way that potentially provides a unique signal [30–32].

It is also possible that the energy density due to rotation remains subdominant to the thermal bath. As we will see, in this case the temperature T_S where the saxion reaches its minimum is still of significance for determination of the baryon asymmetry, as it marks the time where $\dot{\theta}$ changes its scaling. However, this temperature would no longer mark the onset of a kination era because radiation remains dominant.

We now comment on the possibility that saxion thermalization is late so that the saxion comes to dominate the energy density of the universe. We define the ratio r of the axion rotation to the saxion oscillation energy densities, which is in turn determined by the ratio of the potential gradients between the angular and radial modes,

$$r \equiv \frac{\rho_\theta}{\rho_S} \simeq \frac{A}{m_S}. \quad (2.12)$$

This r is inversely related to the ellipticity of the initial motion and $r = 1$ corresponds to nearly circular rotations. Here it is assumed that the angular direction is not accidentally

close to the minimum of the potential in Eq. (2.5); otherwise r becomes smaller than A/m_S . The thermal bath created from the saxion is at a temperature T_{th} upon completion of thermalization. This fact allows us to predict T_{RM} because $\rho_S \times r = \rho_\theta$ should hold at T_{th} . This gives $\frac{\pi^2}{30}g_*T_{\text{th}}^4 \times r = \frac{\pi^2}{30}g_*T_{\text{RM}}^4(T_{\text{th}}/T_{\text{RM}})^3$, or equivalently,

$$T_{\text{RM}} = rT_{\text{th}} \quad (\text{for saxion domination}). \quad (2.13)$$

2.2. Kinetic misalignment and production of axion dark matter

In the conventional misalignment mechanism, the value of the axion field is initially frozen by Hubble friction. But once $3H < m_a(T)$, the axion field begins to oscillate around the minimum of its potential. In the axiogenesis framework, on the other hand, the axion is not frozen, rather the PQ field is already rotating with high velocity. This qualitatively changes the dark matter production story. The kinetic misalignment mechanism (KMM) occurs when the kinetic energy of the axion field is greater than the potential energy. The KMM delays the oscillations around the minimum of the potential. In fact, via parametric resonance [33–37], the axion rotation fragments into fluctuations around the QCD confinement scale in this scenario; this effect was noted in the context of axion monodromy in Refs. [38–41]. The axions generated in this way are relativistic upon production with momenta determined by the resonance peak $k_a \simeq \dot{\theta}/2$. With this, we can estimate the yield of the axion as [9, 42]

$$Y_a \simeq \frac{\rho_\theta}{s\dot{\theta}/2} = \frac{\dot{\theta}f_a^2}{s}. \quad (2.14)$$

The axion yield is equal to the charge yield associated with rotation Y_θ . The present day axion energy density is given by $m_a Y_a$. Setting this equal to the observed dark matter abundance $\rho_{\text{DM}}/s \simeq 0.44 \text{ eV}$, allows us to determine the required charge yield,

$$Y_{\theta, \text{KMM}} \simeq 70 \left(\frac{f_a}{10^9 \text{ GeV}} \right), \quad (2.15)$$

the required temperature T_S at which the axion settles to its minimum using Eq. (2.9),

$$T_{S, \text{KMM}} \simeq 1.6 \times 10^6 \text{ GeV} \left(\frac{N_{\text{DW}}}{3} \right)^{\frac{1}{3}} \left(\frac{m_S}{10 \text{ TeV}} \right)^{\frac{1}{3}} \left(\frac{f_a}{10^9 \text{ GeV}} \right)^{\frac{1}{3}} \left(\frac{g_{\text{MSSM}}}{g_*(T_S)} \right)^{\frac{1}{3}}, \quad (2.16)$$

and the temperature at the transition from radiation to matter domination using Eq. (2.10)

$$T_{\text{RM,KMM}} \simeq 2.9 \times 10^6 \text{ GeV} \left(\frac{m_S}{10 \text{ TeV}} \right) \left(\frac{f_a}{10^9 \text{ GeV}} \right) \left(\frac{N_{\text{DW}}}{3} \right). \quad (2.17)$$

3. COMPUTATION OF THE BARYON ASYMMETRY

In this section, we describe the computation of the baryon asymmetry in lepto-axiogenesis.

3.1. Basics of lepto-axiogenesis

The axion rotation couples to the thermal bath via the gluon in the KSVZ theory and via the Higgs fields in the DFSZ theory. The PQ-charge is transferred to a particle-antiparticle asymmetry of particles in the thermal bath, and in equilibrium the charge asymmetry in the bath is of the order of $\dot{\theta}T^2$ [16]. The total $B - L$ charge vanishes in the absence of $B - L$ violation, and the baryon asymmetry is fixed at the electroweak phase transition [10].

The $B - L$ symmetry is broken if the observed non-zero neutrino mass is explained by a Majorana mass term. We consider the Majorana mass given by the Weinberg operator [22], whose supersymmetrization is given by the superpotential

$$W_\nu = c_{ij} \frac{(L_i H_u)(L_j H_u)}{2\Lambda}, \quad (3.1)$$

which can be UV-completed by the seesaw mechanism [43–46]. This operator gives rise to neutrino mass terms, in terms of the vacuum expectation value v_{H_u} of the up-type Higgs field with $v_{H_u}^2 + v_{H_d}^2 \simeq (174 \text{ GeV})^2$,

$$m_\nu^{ij} = \frac{c_{ij} v_{H_u}^2}{\Lambda}, \quad (3.2)$$

related to eigenvalues through the Pontecorvo–Maki–Nakagawa–Sakata (PMNS) matrix

$$U_{\text{PMNS}}^T m_\nu U_{\text{PMNS}} = \text{diag}(m_1, m_2, m_3). \quad (3.3)$$

The Weinberg operator will transfer the particle-antiparticle asymmetry of L_i and H_u to $B - L$ through scattering between the lepton and Higgs fields (and their superpartners) in the

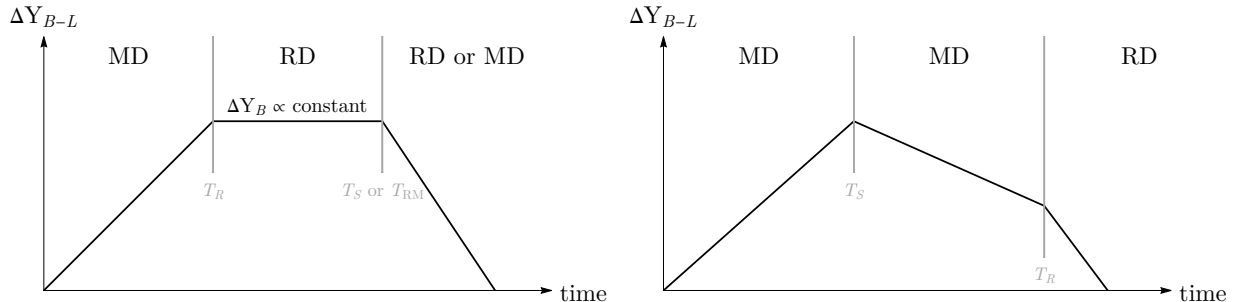


FIG. 2. The baryon minus lepton asymmetry produced per Hubble time ΔY_{B-L} as a function of time in log-log scales during radiation-dominated and matter-dominated eras. Relevant temperatures are labeled in gray and corresponding cosmological eras are labeled in black.

bath. The scattering is not in equilibrium for temperatures $T \lesssim 10^{12} \text{ GeV} \times (0.03 \text{ eV}/m_\nu)^2$, so the transfer of the PQ charge to $B - L$ is suppressed by a factor of Γ_L/H with Γ_L the lepton-number violating rate. That is, $B - L$ asymmetry is produced by a “freeze-in” process [10]. This $B - L$ asymmetry is ultimately further processed by electroweak sphalerons to give a baryon asymmetry $n_B \simeq (28/79)n_{B-L}$ [47].

To calculate the rate of $B - L$ asymmetry production, we must account for all scattering processes due to the operator in Eq. (3.1). Each contribution takes the form

$$\dot{n}_{B-L} \supset 2 \int d\Pi_a d\Pi_b d\Pi_c d\Pi_d e^{-\frac{E_a+E_b}{T}} \left(e^{\frac{\mu_a}{T} + \frac{\mu_b}{T}} - e^{\frac{\mu_c}{T} + \frac{\mu_d}{T}} \right) (2\pi)^4 \delta^{(4)}(p_a + p_b - p_c - p_d) |\mathcal{M}|^2, \quad (3.4)$$

where a, b, c , and d are field labels, momenta $\{p_a, p_b\}$ are incoming and $\{p_c, p_d\}$ are outgoing, and $d\Pi_X \equiv \frac{1}{(2\pi)^3} \frac{d^3 p_X}{2E_X}$ with E_X the energy of field X . The initial factor of two is because the processes have $\Delta L = 2$. Here, μ_X is the chemical potential of field X . See the Appendix of Ref. [14] for discussion in a similar context. For chemical potentials much smaller than temperature, the sum over all scattering processes gives

$$\dot{n}_{B-L} = \frac{72}{\pi^5} T^5 \sum_i \sum_j \left| \frac{c_{ij}}{2\Lambda} \right|^2 \left[\frac{1}{2} (\mu_{\ell_i} + \mu_{\ell_j}) + \mu_{\tilde{H}_u} + \mu_\lambda \right], \quad (3.5)$$

with i and j running over the three generations. We have assumed that processes involving scattering between Higgsinos \tilde{H}_u , gauginos λ , and Higgs bosons are in equilibrium (and similarly for sleptons), which is typically the case. We have included scattering processes

involving superpartners, which were neglected in Ref. [16]. We also go beyond the one-generation approximation used there; this has a smaller effect. We have also assumed that the masses of ℓ and H_u are smaller than T . As we will discuss in Sec. 3.3, this is not true for the DFSZ model for sufficiently high temperatures, since a large field value of S may impart a mass $> T$ to H_u and H_d .

The coefficient of the Weinberg operator can be related to the neutrino masses and mixings as in Eqs. (3.2) and (3.3), so the production rate of the $B - L$ asymmetry may be recast as

$$\dot{n}_{B-L} = \sum C_i(T) m_{\nu_i}^2 \frac{\dot{\theta} T^5}{v_{H_u}^4}, \quad (3.6)$$

where m_{ν_i} is the i^{th} neutrino mass eigenvalue. The coefficients $C_i(T)$ (which are in general a function of PMNS mixing) are determined by calculating the relevant chemical potentials. Their values depend on what interactions are in equilibrium at a given temperature as well as the choice of axion model. Results for $C_i(T)$, generally of order 10^{-2} – 10^{-3} , and the details of their computation are given in Appendix A. The yield of the $B - L$ asymmetry produced per Hubble time may then be estimated as

$$\Delta Y_{B-L} \simeq \frac{\dot{n}_{B-L}}{sH} = \left(\frac{45}{2\pi^2 g_*} \right) \sum C_i(T) m_{\nu_i}^2 \frac{\langle \dot{\theta} \rangle T^2}{H v_{H_u}^4}, \quad (3.7)$$

with $\langle \dot{\theta} \rangle$ the time average of $\dot{\theta}$.

During radiation domination, $H \propto T^2$, so for $T > T_S$, where $\langle \dot{\theta} \rangle \simeq N_{\text{DW}} m_S$ is a constant [16], the temperature dependence of ΔY_{B-L} in Eq. (3.7) is especially simple. It is independent of the temperature, except for a small implicit dependence through the determination of C_i . On the other hand, ΔY_{B-L} decreases with temperature after $T < T_S$ because then $\dot{\theta} \propto T^3$. The scaling of ΔY_{B-L} during different epochs is summarized in Table IV in Appendix B, and is illustrated in the left panel of Fig. 2.

An era of constant ΔY_{B-L} indicates a logarithmic enhancement in the integrated production of Y_{B-L} . For the case of a long radiation-dominated era, we derive the expression

of the final asymmetry Y_{B-L} by integrating \dot{n}_{B-L}/s over time from T_i to T_f using Eq. (3.6),

$$Y_{B-L} = \int \frac{\dot{n}_{B-L}}{s} dt = - \int_{T_i}^{T_f} \frac{\dot{n}_{B-L}}{sHT} dT, \quad H = \sqrt{\frac{\pi^2 g_*}{90}} \frac{T^2}{M_{\text{Pl}}}. \quad (3.8)$$

We obtain an analytic result

$$Y_{B-L} = \left(\frac{90}{\pi^2 g_*} \right)^{\frac{1}{2}} \left(\frac{45}{2\pi^2 g_*} \right) \sum C_j m_{\nu_j}^2 \frac{M_{\text{Pl}} N_{\text{DW}} m_S}{v_{H_u}^4} \ln \left(\frac{T_i}{T_f} \right) \quad \text{for } T_i \gg T_f, \quad (3.9)$$

where T_i and T_f mark the initial and final temperatures of the era when ΔY_{B-L} is a constant. Reproducing the observed baryon asymmetry, $Y_B^{\text{obs}} = 8.7 \times 10^{-11}$ [48], requires a saxion mass

$$m_S \simeq 135 \text{ TeV } N_{\text{DW}}^{-1} \left(\frac{g_*}{g_{\text{MSSM}}} \right)^{\frac{3}{2}} \left(\frac{0.01 \times 0.005 \text{ eV}^2}{\sum C_j m_{\nu_j}^2} \right) \left(\frac{7}{\ln \left(\frac{T_i}{T_f} \right)} \right). \quad (3.10)$$

For $T > T_R$ (or for $T < T_{\text{RM}}$), the universe is not radiation-dominated, and production becomes IR (or UV)-dominated. Again, this is summarized in Table IV and illustrated in the left panel of Fig. 2.

If the reheat temperature is lower than the temperature where the saxion settles to its minimum, i.e., $T_R < T_S$, then Eq. (3.9) does not hold because $\dot{\theta}$ is never constant during the radiation domination era, instead $\dot{\theta} \propto T^3$. In this case, $B-L$ production peaks at T_S , which is illustrated in the right panel of Fig. 2. Then, the asymmetry may be obtained by first computing the redshift-invariant quantity $\dot{n}_{B-L}/(H\rho_{\text{inf}})$, with the inflaton energy density denoted by ρ_{inf} . This quantity is readily evaluated at T_S , see Eq. (3.6), recalling that $|\dot{\theta}| \simeq N_{\text{DW}} m_S$ at this time. Then we can normalize the quantity to n_{B-L}/s at T_R :

$$Y_{B-L} = \frac{\dot{n}_{B-L}}{H\rho_{\text{inf}}}\Big|_{T=T_S} \times \frac{\rho_{\text{inf}}}{s}\Big|_{T=T_R} = \left(\frac{90}{\pi^2 g_*} \right)^{\frac{1}{2}} \left(\frac{45}{2\pi^2 g_*} \right) \sum C_i m_{\nu_i}^2 \frac{M_{\text{Pl}} N_{\text{DW}} m_S}{v_{H_u}^4} \left(\frac{T_R}{T_S} \right)^7, \quad (3.11)$$

where we have assumed inflationary reheating by perturbative decays of the inflaton so $H(T) = H(T_R) \times (T/T_R)^4$ for $T > T_R$.

The result depends on the choice of the neutrino spectrum. We will show results for a normal hierarchy (NH), or inverted hierarchy (IH), assuming the lowest mass eigenvalue is negligible, so the overall mass scale is given by the mass differences determined by oscilla-

tions. Even if we saturate the upper bound $\sum m_\nu < 0.12$ eV from the Cosmic Microwave Background along with data from Baryon Acoustic Oscillations [48], the predictions for this case are not so different from those of the inverted hierarchy case. Precisely speaking, the values of $\sum C_i m_{\nu_i}^2$ with the upper bound saturated are 8% (normal hierarchy) and 16% (inverted hierarchy) larger than that for the inverted hierarchy with a negligible lightest neutrino mass.

3.2. KSVZ

The KSVZ model includes a coupling

$$W_{\text{KSVZ}} = \lambda_\Psi P \bar{\Psi} \Psi \quad (3.12)$$

with Ψ a new colored quark charged under the PQ symmetry such that charges $PQ_\Psi + PQ_{\bar{\Psi}} + PQ_P = 0$. This coupling is the origin of the mixed PQ-QCD anomaly which allows the axion to solve the strong CP problem. The λ_Ψ coupling plays an important role in the thermalization of the rotation.

The KSVZ model was carefully examined in Refs. [16, 17]. We refer readers to these references for details, including the thermalization of the rotating PQ field. Here we focus on the implications of a factor of six enhancement in the baryon asymmetry production efficiency compared to Ref. [16]. This factor of six is the result of supersymmetrizing the Weinberg operator in Eq. (3.1), allowing lepton asymmetry production from scattering involving superpartners. This factor is independent of the UV completion of the axion and applies to the DFSZ case as well. The existence of superpartners in the bath also changes the efficiency of baryon asymmetry production by affecting the equilibrium Boltzmann equations and conserved quantities given in Appendix A.

As a benchmark, the observed baryon asymmetry is reproduced for a saxion mass

$$m_S \simeq 190 \text{ TeV} \left(\frac{1}{N_{\text{DW}}} \right) \left(\frac{g_*}{g_{\text{MSSM}}} \right)^{\frac{3}{2}} \left(\frac{0.0106 \times 0.005 \text{ eV}^2}{\sum C_j m_{\nu_j}^2} \right) \left(\frac{5.3}{\ln \left(\frac{T_i}{T_f} \right)} \right) \quad (\text{KSVZ}), \quad (3.13)$$

where we use $C_i = 0.0106$ based on Table III. In the determination of C_i , we have gone

beyond the one-generation approximation of Ref. [16]. This value of $C_i = 0.0106$ applies when the anomaly coefficients for the weak and strong interaction are identical $c_W = c_g (= 1)$ and when all Yukawa couplings are in equilibrium. To get the benchmark value 5.3, we take $T_i = T_R = 2 \times 10^9$ GeV and $T_f = T_{\text{RM}} = 10^7$ GeV.

3.3. DFSZ

In the DFSZ case, the effective μ -term depends upon the value of the scalar field. This effective μ -terms arises from the superpotential coupling

$$W_\mu = \lambda \frac{P^n H_u H_d}{M^{n-1}}. \quad (3.14)$$

The idea of relating the μ -term to the scale of Peccei-Quinn symmetry is sometimes known as the Kim-Nilles mechanism, which was originally explored for the $n = 2$ case in [49]. Because the value of P changes during the universe's history, so too will the masses of the Higgs fields. As discussed below, this can impact the way in which the lepton asymmetry is transferred to the bath via Eq. (3.1).

The superpotential of Eq. (3.14) gives a temperature dependent $\mu(T) = \lambda P^n / M^{n-1}$. At temperatures before P settles to its minimum, this scales as $R^{-3n/2}$, which is proportional to $T^{3n/2}$ during radiation domination. We define a temperature T_μ at which the temperature and the effective $\mu(T)$ are equal,

$$T_\mu = \left(\frac{T_S^{3n/2}}{\mu} \right)^{\frac{1}{3n/2 - 1}} = \begin{cases} 10^9 \text{ GeV} \left(\frac{T_S}{100 \text{ TeV}} \right)^3 \left(\frac{\text{TeV}}{\mu} \right)^2 & \text{for } n = 1 \\ 10^6 \text{ GeV} \left(\frac{T_S}{100 \text{ TeV}} \right)^{\frac{3}{2}} \left(\frac{\text{TeV}}{\mu} \right)^{\frac{1}{2}} & \text{for } n = 2 \end{cases}, \quad (3.15)$$

where μ is the present-day value to which $\mu(T)$ settles for temperatures below T_S . For temperatures $T > T_\mu$, scattering via the Weinberg operator is ineffective as the lepton-number violation is limited to even higher dimension operators generated by integrating out the Higgs superfields.

So, the earliest temperature at which the chiral asymmetry may be effectively transferred to $B - L$ is T_μ . However, the reheat temperature T_R is sometimes limited by BBN constraints [23, 24] to values that are smaller than T_μ . In this case, the earliest temperature

relevant for transfer to $B - L$ is T_R . Based on Eq. (3.10) and $N_{\text{DW}} = 3n$, a benchmark prediction of the saxion mass is

$$m_S \simeq 39 \text{ TeV} \times \left(\frac{1}{n}\right) \left(\frac{g_*}{g_{\text{MSSM}}}\right)^{\frac{3}{2}} \left(\frac{0.0153 \times 0.005 \text{ eV}^2}{\sum C_j m_{\nu_j}^2}\right) \left(\frac{5.3}{\ln\left(\frac{T_i}{T_f}\right)}\right) \quad (\text{DFSZ}). \quad (3.16)$$

To get the benchmark value of 5.3 in the parentheses, we have taken $T_i = T_R = 2 \times 10^9 \text{ GeV}$ and $T_f = T_S = 10^7 \text{ GeV}$. The benchmark value of C_i corresponds to the case where all Yukawa interactions and the gaugino mass are in equilibrium; see Table II in the Appendix.

The saxion mass, which we assume to be of the same order as the soft scalar masses of the MSSM, may be $\mathcal{O}(10) \text{ TeV}$; this is consistent with the observed Higgs boson mass if the ratio of the Higgs field vacuum expectation values $\tan \beta \gg 1$. Larger m_S is also possible, which could reproduce the Higgs boson mass for more modest values of $\tan \beta$.

4. DETAILED ANALYSIS OF THE DFSZ MODEL

We now analyze the DFSZ model in detail. We discuss the thermalization of P via the coupling with the Higgs superfields in Eq. (3.14). We then show the allowed parameter space, determining both the minimum values of m_S consistent with the generation of the baryon asymmetry and also the values of m_S predicted by the production of both the baryon asymmetry and the dark matter abundance. We analyze the cases where the asymmetry is generated during reheating or the subsequent radiation-dominated era and the case where the saxion eventually dominates the energy. We discuss complications that may arise from the possible fragmentation of the rotation into Q-balls and explain how they can be avoided.

4.1. Thermalization

If the saxion does not thermalize sufficiently early, it will come to dominate the energy density of the universe. In this case, when it ultimately decays, it will produce entropy which can dilute the baryon asymmetry.

We assume that the dominant interactions of the saxion are via the coupling in the superpotential that gives the effective μ -term, Eq. (3.14). Then the saxion can be thermalized

via its interaction with the Higgsino at a rate given by

$$\Gamma_{S\tilde{H}\tilde{H}} \simeq 0.1 \frac{\mu^2(T + m_S)}{S^2} \left(\frac{S}{N_{\text{DW}} f_a} \right)^{2n}, \quad (4.1)$$

where the term with T or m_S corresponds to the scattering or the decay rate, respectively.

For $n = 1$, the rate is independent of the evolution of the saxion field value S . The thermalization temperature is found by setting this rate equal to $3H$, and is given by

$$T_{\text{th}} \simeq \left(\frac{90}{\pi^2 g_*} \right)^{\frac{1}{2}} \frac{\mu^2 M_{\text{Pl}}}{30 N_{\text{DW}}^2 f_a^2} \simeq 200 \text{ TeV} \left(\frac{\mu}{\text{TeV}} \right)^2 \left(\frac{10^8 \text{ GeV}}{f_a} \right)^2 \left(\frac{3}{N_{\text{DW}}} \right)^2 \left(\frac{g_{\text{MSSM}}}{g_*(T_{\text{th}})} \right)^{\frac{1}{2}}, \quad (4.2)$$

which is valid for $T_{\text{th}} \gg m_S$, often the case for parameters of interest. The above expression assumes radiation domination. If the reheat temperature is below this T_{th} , thermalization instead occurs during the period of inflationary reheating, and the actual thermalization temperature becomes lower than that in Eq. (4.2) (but above T_R) due to an enhanced Hubble rate with respect to that for radiation domination. However, thermalization of the saxion during inflationary reheating will not create more entropy than already created by the inflaton. So, the precise value T_{th} will be irrelevant; instead, the value of T_R will be important for analysis of the baryon asymmetry.

For $n > 1$ and $S > N_{\text{DW}} f_a$, the thermalization rate depends on S , so we need the scaling of S with temperature. Conservation of S number implies that S scales as $R^{-3/2}$. During radiation domination, $R \propto T^{-1}$, so $\Gamma_{S\tilde{H}\tilde{H}} \propto (T + m_S) S^{2n-2} \propto (T + m_S) T^{3n-3}$ increases with increasing T faster than a radiation-dominated $H \propto T^2$ does for any $n > 1$. Therefore, for $n > 1$ the saxion may thermalize at a high temperature but then decouple from the thermal bath when $\Gamma_{S\tilde{H}\tilde{H}}$ drops below the Hubble expansion rate. However, there is a maximum temperature at which the saxion can thermalize via Higgsino scattering, namely $T \sim T_\mu$. Above this temperature, Higgsinos are out of equilibrium because their mass exceeds the temperature. To test whether thermalization occurs at this point, we equate $\Gamma_{S\tilde{H}\tilde{H}}|_{T=T_\mu} = 3H(T_\mu)$. Using Eq. (3.15), for $n = 2$ we find that T_S drops out from this relation, and the following constraint on f_a may be derived

$$f_a \lesssim 2 \times 10^9 \text{ GeV} \left(\frac{\mu}{10 \text{ TeV}} \right)^{\frac{1}{2}} \left(\frac{g_{\text{MSSM}}}{g_*(T_\mu)} \right)^{\frac{1}{4}} \left(\frac{6}{N_{\text{DW}}} \right) \quad (n = 2). \quad (4.3)$$

For f_a larger than this critical value, the coupling of saxion is too weak to thermalize at T_μ . Instead, thermalization waits until after T_S and occurs at the lower T_{th} given in Eq. (4.2). For low inflationary reheat temperatures (or the case where the saxion comes to dominate), this critical value Eq. (4.3) is modified due to an enhanced Hubble expansion rate and a different scaling of S with respect to temperature during a matter-dominated era. The inflaton- and saxion-dominated cases will be discussed in Sec. 4.2.2 and Sec. 4.3.2, respectively.

Another possible thermalization channel is via the saxion scattering with the W gauge boson. This occurs with a rate given by

$$\Gamma_{SWW} = n^2 \times b \frac{T^3}{S^2}, \quad (4.4)$$

where $b \simeq 10^{-5}$ [50–52]. Even when the saxion- W scattering does not completely thermalize the saxion, such scattering can play an important role in generating the thermal bath necessary for the Higgsinos to thermalize the saxion. This will be discussed in Sec. 4.3.2.

4.2. No saxion domination

The analysis of baryon asymmetry and dark matter production from axion rotations depends on whether the saxion comes to dominate the energy density and creates entropy upon its thermalization. In this section, we focus on the case where the saxion is thermalized sufficiently early so this does not occur. Then, for much of the parameter space, the baryon asymmetry production dominantly occurs during the radiation domination era following inflationary reheating. We also consider the possibility that the dominant production occurs during inflationary reheating, which can happen for low reheat temperatures. The case with saxion domination is analyzed in Sec. 4.3.

4.2.1. $n = 1$

In this section we give results for the $n = 1$ case, where the μ -term arises through a renormalizable coupling defined in Eq. (3.14). First, we discuss whether both the baryon asymmetry and dark matter may be generated by the dynamics of the axion field. In this $n = 1$ case, consistency with bounds on the axion decay constant from red giant cooling significantly constrains the ability to simultaneously realize the baryon asymmetry and axion

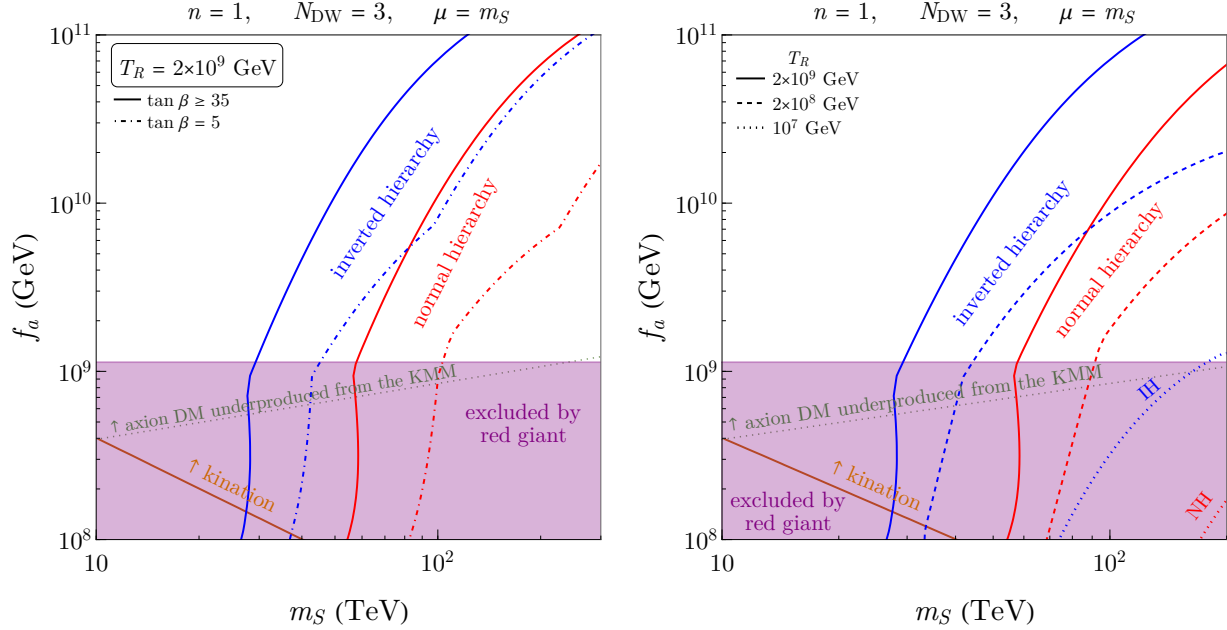


FIG. 3. Minimum m_S for $n = 1$, domain wall number $N_{\text{DW}} = 3$, and $\mu = m_S$. The baryon asymmetry can be correctly reproduced on and to the right of (blue/red) lines with the associated cosmology described in (II) and (III). Different colors distinguish the assumed neutrino mass spectra. In the left panel with $T_R = 2 \times 10^9$ GeV, solid curves are valid for all $\tan \beta \geq 35$, while dot-dashed curves correspond to $\tan \beta = 5$. In the right panel, the solid, dashed, and dotted line styles indicate reheat temperatures $T_R = 2 \times 10^9$ GeV, 2×10^8 GeV, 10^7 GeV. The effects of $\tan \beta$ and T_R are described in (III). Above the green dotted line, as discussed in (I), kinetic misalignment underproduces axion dark matter. The possibility of generating sufficient dark matter using a larger μ is discussed in (IV) with results shown in Fig. 5. The purple region is excluded by observations of red giants [53, 54].

dark matter. The generation of dark matter is discussed in (I) below. Then, independent of the origin of dark matter, we focus on the determination of the lowest scale of supersymmetry breaking consistent with the successful generation of the baryon asymmetry. In (II) we outline how to find this minimum scale. In (III) we present results, including the dependence on $\tan \beta$ and the reheat temperature T_R . Finally, drawing from the knowledge from (III), we present and discuss the parameter space for achieving both the baryon asymmetry and axion dark matter in (IV), including the effects of the reheat temperature.

(I) Axion dark matter? Below the green dotted line in Fig. 3, the dark matter abundance would be successfully explained by the kinetic misalignment mechanism. Above the green dotted line, axion dark matter is necessarily underproduced. This is because even the maximum possible charge yield, achieved when the saxion dominates, $Y_\theta = 3rT_{\text{th}}/4N_{\text{DW}}m_S$ with T_{th} given in Eq. (4.2), is too low to provide axion dark matter. Low values of f_a in the

purple shaded region of Fig. 3 are excluded by red giant brightness observations that bound axion-electron couplings [53, 54]. The incompatibility of these regions shows that generation of all of the dark matter is not possible with the parameters shown. Here we have assumed $\mu = m_S$. Higher values of μ relative to m_S shift this green dotted line upward, eventually allowing compatibility with the bound. We discuss this possibility further in (IV).

Moreover, if additional thermalization channels beyond those described in Sec. 4.1 are present, then it would be possible to increase T_{th} and hence the maximal yield. This could allow the KMM to reproduce the observed DM abundance for larger f_a ; see Ref. [8].

Here, we do not include such channels. So, above this green line, an additional source of dark matter would be required. We assume that whatever produces the balance of the dark matter budget does not disturb the prediction of the baryon asymmetry. This would be the case, for example, if the dark matter were produced by thermal freeze-out of an LSP.²

(II) Finding the minimum m_S : Even in cases where it is impossible to reproduce the full DM abundance, it is nonetheless of interest to understand what sets the minimum superpartner scale m_S consistent with the production of the baryon asymmetry. Since the size of the baryon asymmetry is proportional to $\dot{\theta}$ and hence m_S , this minimum m_S scale can be found by maximizing the baryon asymmetry production efficiency.

The optimal cosmological evolution to obtain the smallest m_S can be obtained as follows. It is best to minimize $T_f = \max(T_S, T_{\text{RM}})$ so the logarithmic enhancement in Eq. (3.9) is maximized, but this should be done while avoiding entropy production that would dilute the asymmetry. Thus, the maximum baryon generation efficiency is achieved if neither the saxion nor the rotation comes to dominate the total energy density. This is accomplished if $T_{\text{RM}} = \min(T_{\text{th}}, T_S)$. This ensures saxion thermalization (which occurs at T_{th}) happens early enough to avoid entropy production. It also ensures that the rapid redshift of the energy of rotation (which begins at T_S) occurs early enough that the rotation does not come to dominate; this will make the radiation-dominated era—and hence the period of logarithmically enhanced baryon production—as long as possible. This procedure also minimizes T_f .

To clarify this cosmological history that produces the maximum asymmetry, we have shown relevant temperatures as functions of f_a for $m_S = 30$ TeV in Fig. 4. The left (right)

² Given the superpartner scales considered here, this might require a hierarchy between gaugino/Higgsino masses and scalar masses. Note, a thermally produced wino LSP would require a cored DM profile to avoid indirect detection bounds, see, e.g. [55, 56].

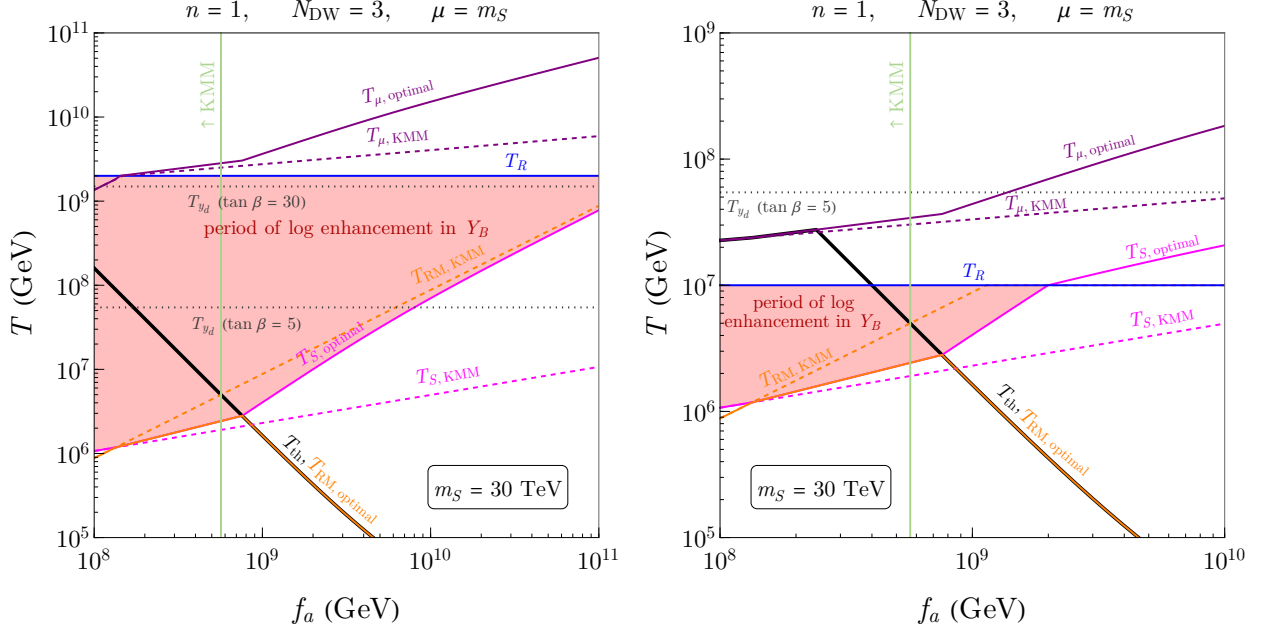


FIG. 4. Cosmologically relevant temperatures as functions of f_a for fixed $m_S = 30$ TeV and $T_R = 2 \times 10^9$ GeV (left panel) and $T_R = 10^7$ GeV (right panel). The red shaded region between the reheat temperature T_R and $\max(T_S, T_{RM})$ indicates the range of temperatures where the dominant baryon asymmetry is produced. During this epoch, the baryon asymmetry produced per Hubble time is constant so the total Y_{B-L} receives a logarithmic enhancement, see Eq. (3.9). The subscript “KMM” refers to values that ensure axion dark matter is produced by the kinetic misalignment mechanism; see Eqs. (2.16) and (2.17) for example. This can be satisfied only to the left of the vertical green line. This corresponds to the region below the green line in Fig. 3. The subscript “optimal” indicates the cosmological scenario where Y_B is most efficiently produced, leading to the smallest required m_S , corresponding to the curve segments above the green dotted line in Fig. 3. The optimal scenario is achieved by choosing the charge yield Y_θ such that $T_{RM, optimal} = \min(T_S, T_{th})$ so as to avoid rotation or saxion domination. For $f_a > 1.5 (7.5) \times 10^8$ GeV, $T_{RM, optimal}$ follows T_S (T_{th}), while $T_{\mu, optimal}$ and $T_{S, optimal}$ change accordingly. Temperatures marked T_{y_d} indicate when interactions involving the down-Yukawa coupling come into equilibrium for different choices of $\tan \beta$; different C_i will apply above and below these lines, see (III). Temperatures denoted T_μ show when Higgsinos come into thermal equilibrium.

panel is for $T_R = 2 \times 10^9$ GeV (10^7 GeV). As discussed above, the optimal scenario for efficient baryon asymmetry production is to choose the PQ charge Y_θ (and hence the energy density in the saxion and rotation) so that $T_{RM} = \min(T_S, T_{th})$. For $f_a > 7.5 \times 10^8$ GeV, this imposes $T_{RM} = T_{th}$, and we refer to this T_{RM} as $T_{RM, optimal}$, according to Eq. (2.13). Once we have fixed T_{RM} in this way, T_S and T_μ may be determined. We have shown these as the $T_{S, optimal}$ and $T_{\mu, optimal}$ curves, which deviate from the values required by the KMM shown in dashed lines.

There is one final minor complication. The region above the orange line in Fig. 3 would

lead to a period of matter domination followed by kination domination had we assumed axion dark matter from the KMM, i.e., $T_{\text{RM,KMM}} > T_{S,\text{KMM}}$ using Eqs. (2.16) and (2.17). However, the goal for Fig. 3 is to derive the minimum m_S rather than requiring the KMM. The optimal choice for T_{RM} to find this minimal m_S is not $T_{\text{RM,KMM}}$, but rather $T_{\text{RM,optimal}} = T_{S,\text{optimal}}$, and this choice is applied in the region between the green dotted and the orange lines in Fig. 3 with $m_S \gtrsim 10$ TeV. This is the case between $f_a = (1.5\text{-}7.5) \times 10^8$ GeV in both panels of Fig. 4, where $T_{\text{RM,optimal}} = T_{S,\text{optimal}}$. This optimal cosmology corresponds to Fig. 1 but with the blue curve shifted downwards and to the left so that the radiation energy density is equal to that of rotation at the kink in the rotation energy density.

(III) Results on minimum m_S : The blue and red curves in Fig. 3 show the minimum values of m_S for which the baryon asymmetry may be achieved, with different colors corresponding to the choice of the neutrino mass spectrum. The solid curves in both panels of Fig. 3 are identical and assume $T_R = 2 \times 10^9$ GeV. Although the dot-dashed curves in the left panel also assume $T_R = 2 \times 10^9$ GeV, they assume a different value of $\tan \beta$, whose effect is to be discussed below. For high T_R such as this, Y_B primarily depends on m_S , and the dependence on T_R is logarithmic because of its role in setting T_i in Eq. (3.9). For these curves in the left panel of Fig. 3, the dependence on f_a is also only logarithmic and enters via its impact on $T_f = T_S$. This explains the nearly vertical segments of the curves starting at low values of f_a . Indeed, starting at the bottom of these curves, we have the baryon asymmetry generated during a radiation-dominated era with a logarithmic enhancement. Moving to larger f_a , it eventually becomes impossible to reproduce the dark matter abundance above the green dotted line as explained in (I). Above this point, the most efficient generation of the asymmetry may be found by ensuring that the saxion does not come to dominate the energy density (and thus generate entropy) as described in (II). Consequently, a kink in the curve develops here because the PQ charge must be such that T_{RM} only occurs at thermalization temperature T_{th} so as to avoid this dilution. For the curve segments below the green dotted line and above the orange line, the PQ yield needs to be chosen in a way such that the rotation does not dominate the energy density either; see discussion in (II).

Effects of $\tan \beta$: The dot-dashed curves in the left panel assume a lower value for $\tan \beta = 5$ than the solid curves. The value of $\tan \beta$ can impact the baryon asymmetry via its effect on the down- and electron-Yukawa couplings. When interactions involving the down- or

electron-Yukawa coupling are out of equilibrium, this may change the chemical potentials and hence $C_i(T)$ in the baryon asymmetry of Eq. (3.7). In constructing Fig. 3, we have used the relevant C_i for each temperature range; see Table II and Appendix A for details. See Fig. 9 for the temperatures at which the Yukawa interactions come into equilibrium. We find that the values of C_i depend most sensitively on whether the down-Yukawa interaction is in equilibrium, and they are relatively insensitive to whether the electron-Yukawa interaction is. In the left panel of Fig. 3, dot-dashed lines assume $\tan\beta = 5$, while solid lines assume down-Yukawa interactions are in equilibrium. The solid lines apply for all $\tan\beta \geq 35$ because the interactions come into equilibrium at temperatures higher than the reheat temperature $T_R = 2 \times 10^9$ GeV assumed in this panel. The dot-dashed lines with lower $\tan\beta$ shift to higher m_S compared to the solid lines with higher $\tan\beta$ because out-of-equilibrium down-Yukawa couplings reduce the coefficients C_i and thus the efficiency in producing Y_B and a larger $\dot{\theta}$ is needed to compensate. All lines in the right panel of Fig. 3 assume that down-Yukawa interactions are in equilibrium, which is valid for $\tan\beta > 10$ (2) in the case of the dashed (dotted) lines with $T_R = 2 \times 10^8$ GeV (10^7 GeV).

Impact of reheat temperature: In Fig. 3, the solid and dot-dashed curves in the left panel and the solid lines in the right panel assume $T_R = 2 \times 10^9$ GeV, whereas the dashed (dotted) lines in the right panel are for $T_R = 2 \times 10^8$ GeV (10^7 GeV). The predictions are affected because the logarithmic enhancement of Eq. (3.9), if present, starts at $T_i = T_R$. It is also possible that for sufficiently low T_R , the baryon asymmetry is dominantly produced during the period of inflationary reheating. We will discuss such effects below after commenting on the constraints from BBN.

A reheat temperature $T_R = 2 \times 10^9$ GeV with $m_S \sim$ TeV requires either i) R -parity violation, ii) a small gravitino mass $m_{3/2} \sim 100$ GeV, or iii) a sneutrino as the next-to-LSP that is nearly degenerate with the gravitino LSP. For $m_{3/2} \gtrsim 7$ TeV the bound on T_R rapidly weakens, so we expect that the dashed and dotted curves are valid without any additional assumptions. See Appendix C for more details on BBN constraints.

As T_R decreases, the generation of the baryon asymmetry is less efficient, and higher values of m_S are needed to reproduce the observed baryon abundance. At minimum, this is because lowering T_R reduces T_i , the onset of the radiation-dominated era that is responsible for the logarithmic enhancement in the generation of the asymmetry in Eq. (3.9). This

explains why the dashed and dotted curves are shifted to higher m_S than the solid curves at low values of f_a . For higher f_a , the curve bends further and becomes a straight line because, although T_{RM} still follows T_{th} , eventually the resultant $T_{S,\text{optimal}}$ exceeds T_R . When this occurs, Y_B is no longer dominantly produced during an radiation-dominated era but rather during inflationary reheating. The logarithmic enhancement disappears, and the baryon asymmetry is diluted by entropy produced from the reheating, as in Eq. (3.11). The result is that the baryon asymmetry is sensitive to T_S and therefore f_a . This cosmological evolution may be clarified by examining the right panel of Fig. 4. There, $T_{S,\text{optimal}}$ can be seen to deviate from $T_{S,\text{KMM}}$ at $f_a \simeq 1.5 \times 10^8$ GeV (when $T_{\text{RM},\text{optimal}}$ starts to track $T_{S,\text{optimal}}$), change its slope at $f_a \simeq 7.5 \times 10^8$ GeV (when $T_{\text{RM},\text{optimal}}$ starts to track T_{th}), and then eventually exceed $T_R = 10^7$ GeV for $f_a \gtrsim 2 \times 10^9$ GeV.

(IV) Results on dark matter: We now focus on the region where axion dark matter can be accounted for by kinetic misalignment, i.e., below the dotted green line in Fig. 3. As can be seen in that figure and explained in (I), if $\mu = m_S$, this possibility is in tension with bounds from observations of red giants. However, if this strict relation between μ and m_S is modified, we find that it is possible to produce dark matter in this way. For larger μ , the saxion thermalization rate in Eq. (4.1) is enhanced and therefore the maximum yield $Y_\theta = 3rT_{\text{th}}/4N_{\text{DW}}m_S$ increases, so the green dotted line in Fig. 3 shifts upward. And for $\mu = 3m_S$, the green line is above the purple boundary for $m_S \gtrsim 30$ TeV, and axion dark matter from kinetic misalignment becomes viable. This benchmark case is shown in Fig. 5. Given the narrow range in m_S of interest there, we improve the precision of the prediction by going beyond the analytic evaluation of Y_B that relies on estimating the production of asymmetry per Hubble time ΔY_B . We instead numerically solve the coupled Boltzmann equations of the inflaton and radiation, while adding an energy component from the axion rotation on top of this background evolution. We numerically integrate $\dot{n}_{B-L}R^3$ using Eq. (3.6) to obtain the baryon asymmetry. We find the predictions of m_S are modified (increased) by up to a factors of two for a fixed T_R using this more sophisticated treatment. In the left (right) panel of Fig. 5, an inverted (normal) neutrino mass hierarchy is assumed, and the predictions are shown by the blue (red) contours. We include contours of T_R to show how the reheat temperature affects the prediction. The brown region is excluded because the required energy density in the complex field P , comprised of contributions from rotation

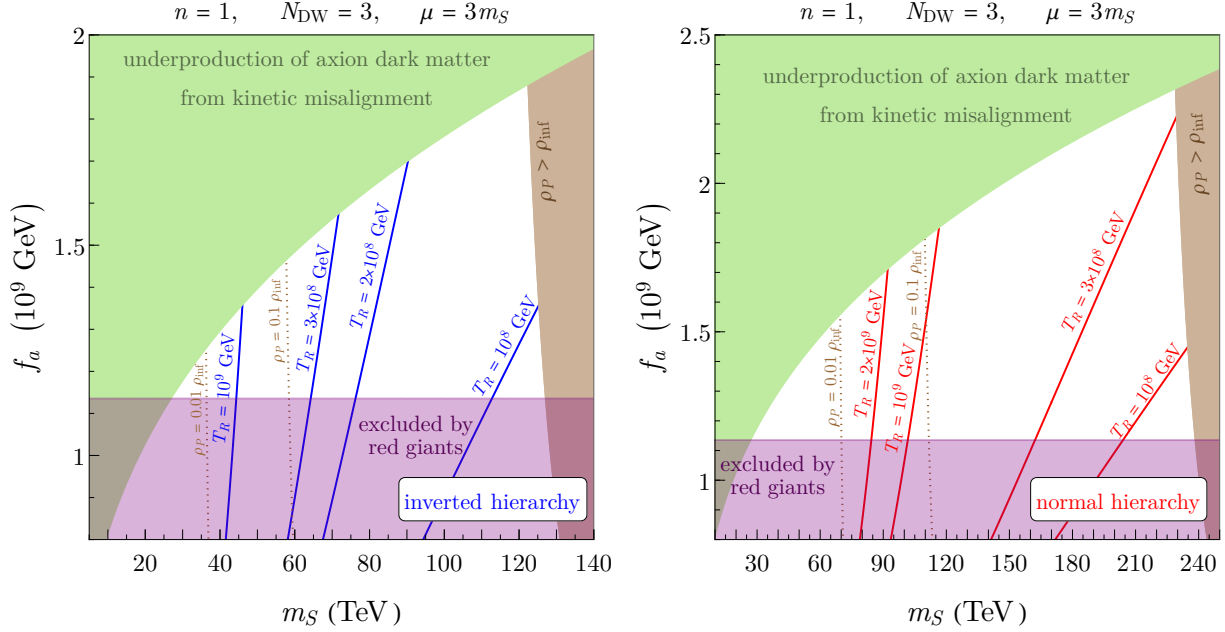


FIG. 5. Parameter space reproducing both the observed dark matter abundance and the baryon asymmetry. The left (right) panel assumes the neutrino mass spectrum with an inverted (normal) hierarchy. The blue and red contours show the reheating temperatures required to reproduce both the baryon asymmetry from leptogenesis and dark matter from kinetic misalignment. The kinetic misalignment mechanism predicts a period of matter domination followed by kination domination in the entire parameter space shown here. The green region leads to underproduction of axion dark matter from kinetic misalignment because of entropy production from saxion domination, i.e., $T_{\text{RM}} > T_{\text{th}}$ using Eqs. (2.10) and (4.2). The purple region is excluded by the red giant brightness observations. The brown region is excluded because the required PQ charge leads to an energy density of the PQ field ρ_P exceeding that of the inflaton, while the brown dotted contours show lower values of ρ_P/ρ_{inf} .

and the saxion $\rho_P \equiv \rho_S + \rho_\theta$ ($\simeq 2\rho_\theta$ for $A \simeq m_S$ according to Eq. (2.12)), exceeds that of the inflaton. The origin of this region may be understood by noting that larger values of m_S require less efficient production of Y_B , which may be achieved by a smaller logarithmic enhancement during radiation domination by decreasing the ratio between T_R and T_{RM} . For fixed T_R , this requires a larger T_{RM} in Eq. (2.10). However, eventually T_{RM} becomes as large as $T_R/2$, at which point $\rho_P \simeq 2\rho_\theta = \rho_{\text{inf}}$, and an inconsistency arises because P would instead drive an epoch of inflation. Two brown dotted curves are shown for $\rho_P/\rho_{\text{inf}} = 0.1$ and 0.01 , which are perhaps more realistic energy densities for P . In summary, the saxion mass is now predicted to have a strict upper limit of 125 (240) TeV for inverted (normal) hierarchy with lower m_S preferred for a realistic ρ_P . This mass range is intriguingly consistent with the supersymmetry-breaking scale determined from the observed value of the Higgs boson mass.

4.2.2. $n = 2$

We now move to the case of $n = 2$ and $N_{\text{DW}} = 6$. Our focus in this case will be on the parameter space where both the baryon asymmetry and dark matter abundance result from the axion rotation. This case is presented in the left panel of Fig. 6 for $\mu = m_S/5$. The blue curve shows the minimum values of m_S compatible with axion dark matter and the baryon asymmetry both arising from axion rotations. This minimum m_S is achieved when T_R is sufficiently high, as discussed below. The blue curve assumes the inverted hierarchy neutrino mass spectra as labeled, while the normal hierarchy case overproduces the baryon asymmetry in this parameter space. We will see that the requirement of the successful generation of both the baryon asymmetry and dark matter prefers a relatively small region of m_S ranging from around 60 TeV to nearly 100 TeV and $f_a = (1-2) \times 10^9$ GeV.

Above the orange line in the left panel of Fig. 6, a period of matter domination followed by kination domination exists because $T_{\text{RM}} > T_{\text{KR}}$. In this case, the era of logarithmically enhanced baryon production ends at T_{RM} , when the matter domination begins. The region above the orange line also gives a potential signal in the modification of primordial gravitational waves [30–32]. This is discussed around Eq. (3.9) and illustrated by the red shaded region in the right panel of Fig. 6. To accurately obtain the final Y_B , rather than using the analytic estimate given in Eq. (3.9), we numerically integrate $\dot{n}_{B-L}R^3$ from T_μ to a temperature much lower than T_{RM} ; this improves the precision of the prediction on m_S and changes the prediction by a factor as large as 2.

In the green shaded region, axions from kinetic misalignment cannot account for all of dark matter because the necessary axion yield $Y_\theta = 3rT_{\text{th}}/4N_{\text{DW}}m_S$ requires a T_{th} value that is higher than can be achieved from saxion-Higgsino scattering given in Eq. (4.2). In particular, above (below) the positively-sloped boundary of the green region, thermalization occurs below (at) T_μ ; see Eq. (4.3). This thermalization condition is also the origin of the vertical green line labeled with KMM in the right panel, which shows various temperatures as functions of f_a for the benchmark point $m_S = 70$ TeV. On the other hand, below the negatively-sloped boundary of the green region, we have $T_{\text{th}} = T_\mu$ and $T_{\text{th}} > T_{\text{RM}}$ so that the saxion does not create entropy upon thermalization. Lastly, as can be seen in the right panel, the era that dominates the production of the baryon asymmetry begins at T_μ , and therefore the result is independent of T_R as long as $T_R > T_\mu$. Using T_μ from Eq. (3.15) and

T_S from Eq. (2.16), one finds $T_\mu \simeq 6 \times 10^7 \text{ GeV} (f_a/10^9 \text{ GeV})^{1/2} (m_S/5\mu)^{1/2}$. The calculated asymmetry will be valid for all T_R larger than this value.

In other words, by lowering T_R , one can explain the baryon asymmetry and dark matter in the region to the right of the magenta line. However, there is a limit on how low T_R can be: in the low T_R and high m_S limits, T_R and T_{RM} approach each other, and when $T_R = 2T_{\text{RM}}$, the energy density of the complex field $\rho_P \equiv \rho_S + \rho_\theta$ is equal to that of the inflaton ρ_{inf} if $A \simeq m_S$, i.e., $\rho_S \simeq \rho_\theta$ based on Eq. (2.12). The resulting upper bound on m_S is shown by the brown line; see a related discussion in Sec. 4.2.1. To the right of this brown curve, $\rho_P > \rho_{\text{inf}}$, which is inconsistent because P would drive inflation. The constraints involving T_R are obtained by calculating Y_B numerically, also including the coupled Boltzmann equations for inflationary reheating.

As the sum of the neutrino masses decreases, both the blue and brown curves will move to the right, so it is possible to reproduce both the baryon asymmetry and the dark matter abundance for all of the white region to the right of the magenta curve. For small enough neutrino mass, the blue curve will reach the intersection of the purple and green regions at the right of the figure, at which point, the window closes.

In summary, simultaneous production of dark matter and the baryon asymmetry is possible between m_S of 60-100 TeV depending on the sum of the neutrino masses, and f_a should lie in the window $(1-2) \times 10^9 \text{ GeV}$. The NH case (with vanishing lowest eigenvalues) is excluded by observations of red giants.

Which neutrino spectra are allowed, however, depends on μ . We have assumed $\mu = m_S/5$ in Fig. 6. Smaller μ would decrease the thermalization rate $\Gamma_{S\tilde{H}\tilde{H}}$. This would make the negatively-sloped boundary of the green region, set by $\Gamma_{S\tilde{H}\tilde{H}} = 3H$ at T_μ , shift downward. The positively-sloped boundary, set by $T_\mu = T_{\text{RM}}$, would shift upward because $T_\mu \propto \mu^{-1/2}$ and $T_{\text{RM}} \propto f_a$. Finally, a small μ increases T_μ and therefore the logarithmic enhancement in Y_{B-L} , which in turn requires a smaller $\dot{\theta} \propto m_S$ to compensate for the increased efficiency in producing Y_{B-L} . This shifts the prediction curves to the left. Numerically, $\mu < m_S/10$ makes the NH case with a vanishing lowest eigenvalue viable for a small range of saxion masses.

We do not analyze the baryon asymmetry in the green shaded region, where axion dark matter is underproduced by kinetic misalignment, because we find that in some of the parameter space the onset of the P rotation can be initiated by the saxion thermal mass.

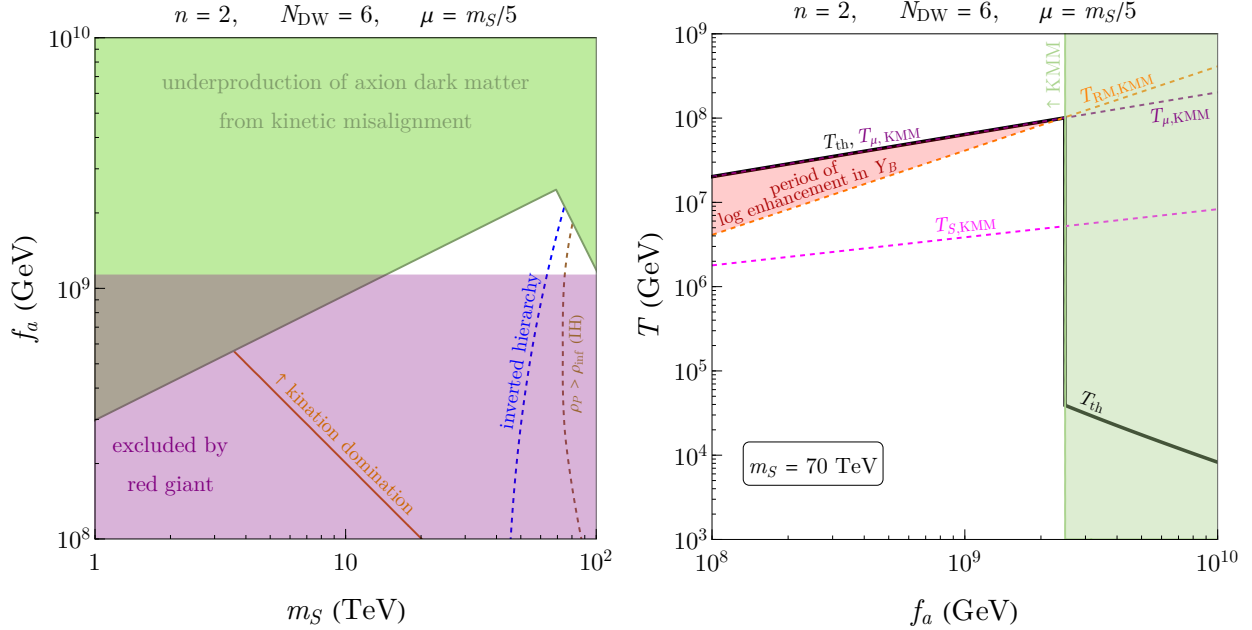


FIG. 6. Analysis of the $n = 2$, $N_{\text{DW}} = 6$ case. **Left:** The baryon asymmetry and the dark matter abundance are correctly reproduced along the blue dashed line for the case of an inverted hierarchy neutrino spectrum, for sufficiently high reheate temperatures. Lower reheate temperatures lead to higher m_S , up to the brown dashed line where the P field starts to drive inflation. In contrast, the normal hierarchy case leads to overproduction of the baryon asymmetry. The purple region is excluded by observations of red giants, while the green region underproduces dark matter. **Right:** Temperatures in this combined dark matter/baryon asymmetry scenario for fixed $m_S = 70$ TeV. The temperature $T_{S,KMM}$ (magenta dashed) indicates where the saxion reaches its minimum. $T_{\mu,KMM}$ indicates the temperature below which the Higgsinos are in thermal equilibrium. T_{RM} (yellow dashed) indicates the temperature where the rotational energy would come to dominate. For low f_a , $T_{S,KMM}$ is reached first, and no era of rotational energy domination occurs. The green shaded region corresponds to the green shaded region in the left panel where the KMM is unable to fully reproduce the dark matter density.

This is because the thermal mass is proportional to μ , which is in turn enhanced at high temperatures by S^{n-1} . Rotations initiated by the thermal mass complicate the determination of the optimal cosmological evolution for the most efficient baryon asymmetry production. The thermal mass also leads to potential formation of Q-balls whose presence makes the baryon asymmetry calculation uncertain; see Sec. 4.5.

4.3. Saxion domination

In this subsection, we discuss a different cosmology where both dark matter and the baryon asymmetry may still be produced by axion rotations. We do not optimize the pro-

duction of the baryon asymmetry nor utilize T_R to explore the parameter space as in Sec. 4.2, but rather study the case where the saxion dominates the energy density before it is thermalized. In this case, the saxion creates entropy that dilutes the baryon asymmetry produced immediately after inflationary reheating. Consequently, the final asymmetry is dominantly produced after saxion thermalization and is therefore independent of the inflationary reheat temperature T_R . The predicted m_S is generically larger than the optimal cases studied in Sec. 4.2 giving the most efficient baryon asymmetry production.

We require both Y_B and dark matter from axion rotations. Then, this scenario makes a prediction for (m_S, f_a) as a function of r , defined in Eq. (2.12) as the ratio of the axion rotation to the saxion oscillation energy densities. The reason for the unique prediction is as follows. For a given μ , the relation $T_{\text{RM}} = rT_{\text{th}}$ from Eq. (2.13) is satisfied along a contour in the (m_S, f_a) plane because T_{RM} and T_{th} are independently determined by (m_S, f_a) . In particular, T_{RM} is given by Eq. (2.10) with Y_θ from kinetic misalignment using Eq. (2.15), and see Sec. 4.1 for discussions of T_{th} for different values of n . Finally, a successful production of Y_B picks out a single point along this contour once the neutrino mass spectrum has been specified. We find that, for $\mu = m_S$, the predicted values of f_a are in tension with red giant bounds except for the normal hierarchy case with $n = 1$ and $r \simeq 1$.

We now comment on the effect of changing μ . If the value of μ is increased, this makes thermalization more efficient and would increase T_{th} . This breaks the relation $T_{\text{RM}} = rT_{\text{th}}$. However, this relation can be restored by going to higher f_a since $T_{\text{RM}} \propto f_a$ and T_{th} decreases with increasing f_a . The predictions for $\mu = 3m_S$ will be shown and discussed.

4.3.1. $n = 1$

The thermalization temperature for $n = 1$ is given in Eq. (4.2). In the saxion domination case, $T_{\text{RM}} = rT_{\text{th}}$ with T_{RM} determined by requiring dark matter from kinetic misalignment, and this gives a relation between m_S and f_a for a given r . Furthermore, to accurately derive Y_B , we numerically solve the coupled Boltzmann equations of the saxion and radiation with the thermalization rate given in Eq. (4.1) and then integrate $\dot{n}_{B-L}R^3$. This then makes a single point prediction (m_S, f_a) when given μ , r , and a neutrino spectrum. The final predictions are shown by the symbols connected by the solid lines in Fig. 7. (The diamonds connected by the dashed black curve are for $n = 2$ and will be discussed below.) The

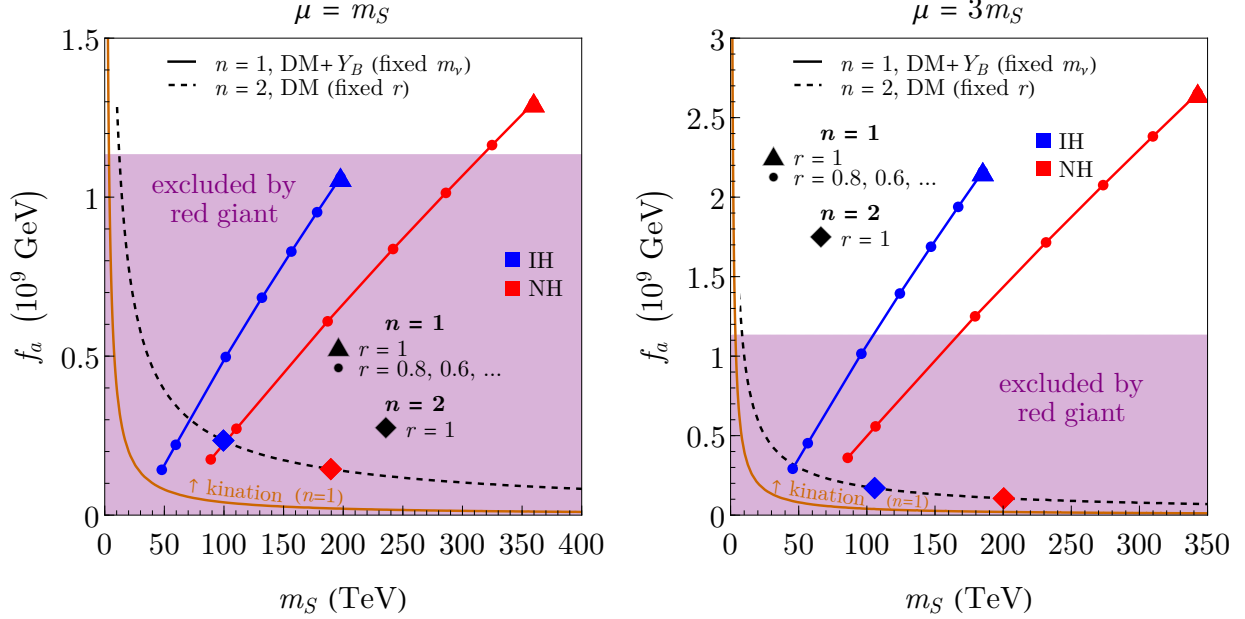


FIG. 7. Predictions for m_S and f_a from the baryon asymmetry via lepto-axiogenesis and axion dark matter from kinetic misalignment in the scenario where the saxion dominates. The left (right) panel is for $\mu = m_S$ ($\mu = 3m_S$). The symbols connected by the solid (dashed) lines are for $n = 1$ ($n = 2$). The triangle and diamond symbols assume the saxion has the same energy as the axion rotation, i.e., $r = 1$ as defined in Eq. (2.12). The circles below triangles denote lower values of r in steps of 0.2 from $r = 0.8$ until $r = 0.02$, after which it is 0.03 and 0.01. The colors refer to the chosen neutrino mass spectrum as labeled. The colored lines connect the predictions of both kinetic misalignment and lepto-axiogenesis for $n = 1$ with various values of r , whereas the dashed black line is the prediction of kinetic misalignment alone for $n = 2$ assuming $r = 1$ (predictions for $n = 2$, $r < 1$ are not included due to complications involving thermalization, see text). In the regions above the orange curves, axion dark matter from kinetic misalignment predicts eras with matter and kination domination, which may leave imprints in primordial gravitational waves [30–32].

triangles at the top are the predictions assuming $r = 1$, while the circles below them show the predictions for smaller r , decreasing in steps of 0.2 until $r = 0.2$, below which the circles are for $r = 0.03$ and $r = 0.01$. The two colors indicate different neutrino mass spectra. The left (right) panel of Fig. 7 shows the predictions for $\mu = m_S$ ($\mu = 3m_S$). The predictions are in a small region with $f_a = (1-3) \times 10^9$ GeV. The required values of m_S range from 100-360 TeV depending upon the choice of neutrino spectrum and are in an interesting range considering the observed Higgs boson mass.

4.3.2. $n = 2$

We continue to analyze the case where the saxion comes to dominate the energy density of the universe before being thermalized, i.e., $T_{\text{RM}} > T_{\text{th}}$, but now for $n = 2$. The results are given in Fig. 7. The diamonds show the points predicted by requiring both the baryon asymmetry and dark matter abundance, which are in tension with the red-giant observations. We nevertheless analyze this $n = 2$ scenario to obtain the prediction from the dark matter abundance (black dashed curves) but with an underproduced baryon asymmetry. The prediction is sharp and points to $m_S \simeq 10$ TeV and $f_a \simeq (1.2-1.3) \times 10^9$ GeV as shown by the black dashed segment above the purple region. The truncation of the black dashed curves at low m_S is due to thermalization constraint discussed below.

The thermalization analysis for $n = 2$ is more involved than for $n = 1$ since $\Gamma_{S\tilde{H}\tilde{H}}$ increases with $(T + m_S)S^{2n-2}$, and thermalization can potentially occur at temperatures higher than T_S when the non-trivial scaling of S may matter. For the saxion to thermalize via scattering with Higgsinos, a thermal bath must be present with a temperature larger than the Higgsino mass parameter $\mu(T) = \mu \times (S(T)/N_{\text{DW}}f_a)^2$. This bath can in principle originate from inflationary reheating or from the saxion scattering with the W gauge boson. In what follows, we assume the high T_R and/or large initial S limit so the inflationary reheating contribution to the bath is negligible around thermalization. (For instance, for the initial S close to the Planck scale, $T_R > \mathcal{O}(10^7)$ GeV is sufficient for this assumption to hold.) The origin of the bath must be from the saxion- W scattering. The temperature of the bath that originates in this way increases [57] during saxion reheating because the temperature dependence of the rate given in Eq. (4.4).

As the temperature increases, it may eventually become equal to the effective $\mu(T)$ at a temperature we call $T_{\text{th},i}$, at which point thermalization via Higgsinos is initiated. Thermalization may then suddenly complete via saxion-Higgsino scattering, and the temperature increases abruptly to T_{th} as the saxion energy is suddenly converted to the bath. This occurs as long as $\Gamma_{S\tilde{H}\tilde{H}} > H$. We assume the saxion field value does not change significantly after thermalization, $S_{\text{th}} \simeq S_{\text{th},i}$, which is the case if the initial rotation is nearly circular ($r \simeq 1$). The temperature right after thermalization T_{th} can be computed by requiring 1) conservation of energy $\rho_S = m_S^2 S_{\text{th},i}^2 = \frac{\pi^2}{30} g_* T_{\text{th}}^4$, 2) initial radiation created by W scattering $\rho_S \frac{\Gamma_{S\tilde{W}\tilde{W}}}{H} = m_S^2 S_{\text{th},i}^2 \frac{\Gamma_{S\tilde{W}\tilde{W}}}{H} = \frac{\pi^2}{30} g_* T_{\text{th},i}^4$ with the subscript “th, i ” indicating evaluation right be-

fore the abrupt thermalization, and 3) the condition for Higgsinos to just come into thermal equilibrium $T_{\text{th},i} = \mu(T_{\text{th},i}) = \mu \times (S_{\text{th},i}/N_{\text{DW}}f_a)^2$. We obtain

$$T_{\text{th}} = 7 \times 10^6 \text{ GeV} \left(\frac{N_{\text{DW}}}{6} \right)^{\frac{1}{3}} \left(\frac{m_S}{20 \text{ TeV}} \right)^{\frac{1}{2}} \left(\frac{m_S}{\mu} \right)^{\frac{1}{6}} \left(\frac{f_a}{6 \times 10^8 \text{ GeV}} \right)^{\frac{1}{3}}. \quad (4.5)$$

Using this expression, we find that along the black dashed line of Fig. 7, the PQ charge yield $Y_\theta = 3rT_{\text{th}}/4N_{\text{DW}}m_S$ matches the value required by the observed dark matter abundance via kinetic misalignment, i.e., Eq. (2.15).

The black dashed line is truncated at low m_S because $\Gamma_{S\tilde{H}\tilde{H}} < H$ when $T = T_{\text{th},i} = \mu(T_{\text{th},i})$. That is to say, even though a bath has been created via saxion-W scattering that allows Higgsinos to come into equilibrium, the interaction rate between Higgsinos and the saxion is still too small to complete thermalization at this time. In this case, only a small fraction, $\Gamma_{S\tilde{H}\tilde{H}}/H$, of the saxion energy density is transferred into the bath at this time. And since $\Gamma_{S\tilde{H}\tilde{H}}$ decreases faster than H when S is still away from the minimum at $N_{\text{DW}}f_a$, thermalization is only possible after S settles to the minimum so that $\Gamma_{S\tilde{H}\tilde{H}} \propto (T + m_S)$ can eventually overtake H . However, in this regime, we find that axion dark matter is underproduced because the low T_{th} gives an insufficient PQ charge $Y_\theta = 3rT_{\text{th}}/4N_{\text{DW}}m_S$.

In deriving this black dashed line, we have assumed $r = 1$. One may be tempted to naively extend the calculation to derive the prediction for lower values of r because r seemingly appears to affect only $S_{\text{th}}/S_{\text{th},i}$. For $r < 1$, $\Gamma_{S\tilde{H}\tilde{H}} \propto S^2$ may first be larger than H when T reaches $T_{\text{th},i}$ but become smaller than H before reaching complete thermalization at T_{th} . The condition $\Gamma_{S\tilde{H}\tilde{H}} > H$ should instead be evaluated at T_{th} with S_{th} rather than at $T_{\text{th},i}$. However, we note that thermalization via Higgsino scattering may be further complicated by the fact that the value of S can get close to the origin in some portion of the cycle when the rotations are very elliptical, $r \ll 1$. During this portion, the saxion-Higgsino scattering may proceed because $T < \mu(S)$ near the origin, while $T > \mu(S)$ when P is far away from the origin. We do not pursue this possibility further.

Finally, we show diamonds along the black dashed line to indicate the prediction from leptogenesis for the different hierarchical neutrino mass spectra. In deriving these predictions, we again numerically solve the coupled Boltzmann equations for the saxion and radiation with a non-trivial thermalization rate scaling and then integrate $\dot{n}_{B-L}R^3$ to obtain the final Y_B . As can be seen in the figure, lower values of f_a are preferred by the predictions,

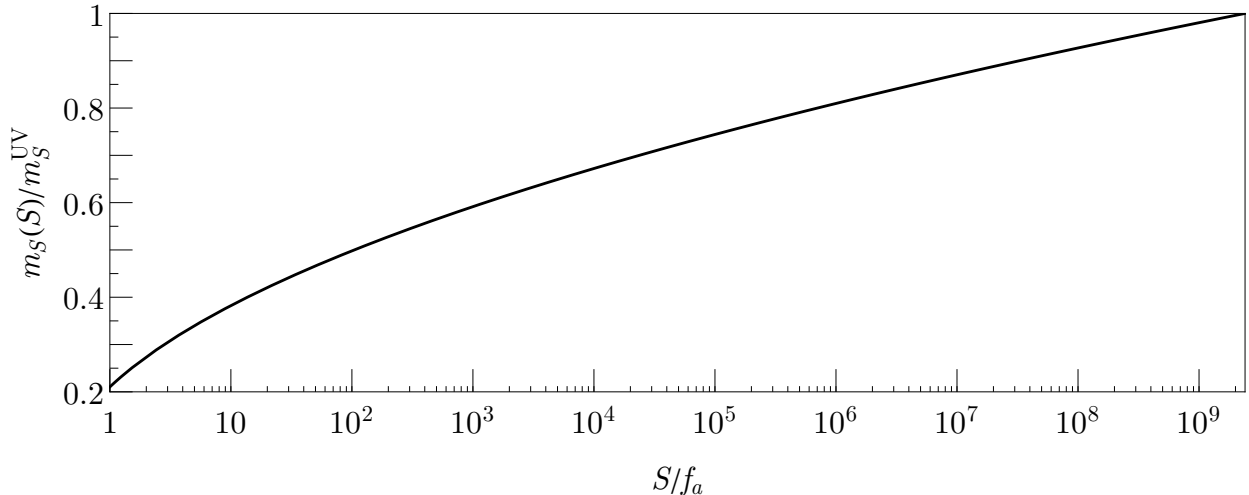


FIG. 8. Curvature of the PQ-field potential normalized to the UV value in the one-field model as a function of the ratio of the field value S to the axion decay constant f_a .

but such low f_a is in tension with the red giant constraints. In fact, even the degenerate limit of the neutrino spectrum leads to underproduction of the baryon asymmetry. Lowering μ may increase the predicted values of f_a , moving towards compatibility with the red-giant bound, but the black dashed line is truncated at lower f_a . As a result, we do not find viable parameter space for a sufficient baryon asymmetry after marginalizing over μ .

4.4. Interpretation of results for one-field model

In this subsection, we re-interpret the results presented in Figs. 3, 5, 6, and 7 for the one-field model defined in Eq. (2.3). This model requires special treatment because, unlike the two-field model of Eq. (2.2), the curvature of the potential in the radial direction is logarithmically enhanced at large field values for S .

In what follows, we define m_S^{UV} as the curvature at $S = M_{\text{Pl}}$. We expect this value to be comparable to other scalar masses in the UV. We will discuss how our earlier results are modified under the understanding that the x -axes of the figures will now refer to m_S^{UV} . We denote $m_S(z)$ as the curvature at lower energy scales; z may refer to the S field value or a temperature to indicate the corresponding field value $S(T)$ at T , i.e., $m_S(T) = m_S(S(T))$. The field dependence of $m_S(S)$ is shown in Fig. 8. Because the change of $m_S(z)$ is only logarithmic, the overall effect on the results is modest. In what follows, we will discuss this effect in detail. Our strategy will be to fix f_a and find the value of m_S^{UV} that would reproduce

the physics of a field-independent m_S in each case.

We begin by discussing the effects of the evolution of $m_S(z)$ on saxion thermalization. The green dotted line in Fig. 3, the green boundary of Fig. 5, and the positively-sloped green boundary of Fig. 6 are all determined by thermalization requirements, and they are set such that $Y_\theta = 3rT_{\text{th}}/4N_{\text{DW}}m_S(T_{\text{th}})$ reproduces the required PQ charge yield $Y_{\theta, \text{KMM}}$ in Eq. (2.15). In Figs. 3 and 5, T_{th} is determined via Eq. (4.2) and scales as the low-energy value of the Higgsino mass squared, μ^2 , which we expect to be $(m_S^{\text{UV}})^2$. Thus, $Y_\theta \propto (m_S^{\text{UV}})^2/m_S(T_{\text{th}})$. For a fixed f_a , we can find the correct value of m_S^{UV} by ensuring $(m_S^{\text{UV}})^2/m_S(T_{\text{th}})$ is equal to the constant m_S of our previous analysis.

Thermalization occurs when the saxion is at (close to) the minimum, for low (high) m_S , as can be seen in Fig. 4. Therefore, $m_S(T_{\text{th}}) \simeq (0.2\text{-}0.5)m_S^{\text{UV}}$ according to Fig. 8, and thus $(m_S^{\text{UV}})^2/m_S(T_{\text{th}}) = (2\text{-}5)m_S^{\text{UV}}$. The green line/region will then shift to the left by a factor of 2-5 to compensate for this. On the other hand, for Fig. 6, the positively-sloped boundaries are in fact unaffected because the condition given in Eq. (4.3) depends on only $\mu \approx m_S^{\text{UV}}$. The negatively-sloped boundaries are set by $T_{\text{th}} = T_{\text{RM}}$, where $T_{\text{th}} = T_\mu$. This condition translates to $m_S(T_{\text{RM}})/(m_S(T_S)/\mu)^{1/2}$ being equal to the m_S derived for the fixed curvature case; this condition has an accidental cancellation numerically so the boundaries do not move appreciably.

We now discuss how the predictions of m_S that reproduce the baryon asymmetry are affected by $m_S(z)$. During the epoch where the ΔY_{B-L} is a constant, the dependence of the total Y_{B-L} on $m_S(T)$ is through a now slightly temperature dependent $|\dot{\theta}(T)| = N_{\text{DW}}m_S(T)$ for $T_i > T > T_f$. For Figs. 3 and 5 ($n = 1$), T_i is T_R and T_f is often T_S (see Fig. 4). For Fig. 6 ($n = 2$), T_i is T_μ , which is not much above T_S , and T_f is often T_S . Since m_S is lower at these lower temperatures compared to m_S^{UV} , the effect is to reduce the efficiency of Y_{B-L} production. To compensate for this, m_S^{UV} needs to increase by a factor of a few. This results in a shift of the prediction curves to the right. As a result of this shift and the left shift of the green dotted line in Fig. 3, the hierarchical cases shown by blue and red curves are more easily compatible with the red giant bound and the green constraint for dark matter. In other words, a viable parameter space for dark matter would open up with a milder hierarchy between μ and m_S than $\mu = 3m_S$ assumed in Fig. 5. The shift would be more prominent in Fig. 6 than Fig. 3 because the former case involves $m_S(T)$ only at temperatures close to T_S .

The brown regions/curves in Figs. 5 and 6 are also affected by a changing m_S . As explained in Secs. 4.2.1 and 4.2.2, these constraints occur because a successful production of Y_B would require $T_{\text{RM}} > T_R/2$, which would result in a period of inflation driven by the saxion. First, as explained above, an evolving $m_S(T)$ decreases the efficiency of production relative to the constant case, so to reproduce the baryon asymmetry, a larger m_S^{UV} is required. Second, because $m_S(T_{\text{RM}})$ is smaller than m_S^{UV} , the saxion will take longer to come to dominate, and so T_{RM} is smaller in the case where the saxion mass evolves. This means the constraint is relaxed, which also shifts the brown regions/curves to higher m_S^{UV} .

Lastly, in Fig. 7, the dominant (logarithmically enhanced) era of asymmetry production is present between T_{th} and $T_{\text{RM}} = rT_{\text{th}}$. For $r = \mathcal{O}(1)$, $T_{\text{RM}} \simeq T_{\text{th}} \gg T_S$, so $m_S(T)$ during this era is $\mathcal{O}(0.5)m_S^{\text{UV}}$, and the predicted points will shift to the right by a factor of 2 or so. The predicted points for $r \ll 1$ are excluded by red giants whether or not we account for the effect of $m_S(z)$.

On balance, for the one-field model, larger values of m_S are preferred than in the two-field case, often by a factor of few.

We discuss the potential domain wall problem in the one-field model. After the initiation but before the thermalization, the rotation is generically not circular. For non-circular motion, fluctuations of the PQ breaking field can be produced by parametric resonance [16, 33–37, 58]. The PQ symmetry may be non-thermally restored by the fluctuations and broken again once the fluctuations are reduced by the expansion of the universe. If this actually occurs, a domain wall-string network is produced, which is stable if $N_{\text{DM}} > 1$ and causes a domain wall problem. Unlike the case without angular momentum [59, 60], it is not clear if the restoration actually occurs, since the non-zero angular momentum provides an effective potential that strongly disfavors the origin of the field space. We leave the investigation of the dynamics via numerical lattice computation to future work, and only note that the one-field model may require $N_{\text{DW}} = 1$ or explicit PQ breaking that can destroy the domain walls $N_{\text{DW}} > 1$ [61].

4.5. Q-balls

If the potential of the S field is nearly quadratic, a small correction may make the potential flatter than a quadratic one, for which a non-topological soliton called a Q-ball

may be formed [62–66]. Q-ball formation can complicate the thermal history. If formed, Q-balls will localize the PQ charge inside them. It is unclear as to what the spatial distribution of the $\dot{\theta}$ will be as the universe evolves in the presence of these Q-balls. This uncertainty would confuse the evaluation of the baryon asymmetry.

Most discussions of Q-balls have taken place in the context of potentials with minima near the origin in field space. It is possible that the symmetry-breaking potential of P allows the Q-balls to decay or even prevents its initial formation. While understanding the dynamics of the Q-balls associated with a symmetry-breaking potential such as the one needed for the axion is of interest, we leave it for future work. For now, we assume that the properties of the Q-balls in the present setup are identical to the more familiar ones associated with potentials that have minima at the origin. We then comment on which cases Q-ball formation might confuse the calculation of the baryon asymmetry, while keeping in mind that future investigations might mitigate these concerns. Histories that include Q-ball formation may actually ultimately prove viable.

For $n = 1$, the thermal potential, given in the second terms of Eqs. (4.6) and (4.8) below, is flatter than a quadratic one for both $\mu(S) > T$ and $\mu(S) < T$, so once Q-balls are formed, they would remain stable until $T \ll m_S$ when the quantum correction to the soft mass of S from interactions with the Higgs fields dominates over the thermal potential. In this case, the estimation of the baryon asymmetry would potentially be rendered invalid, because the Q-balls would be present during the epoch that is important for the generation of the asymmetry. We may avoid the era of a flat potential by coupling P to additional fields, $W = y_\psi P \psi \bar{\psi}$. Because we will require a large y_ψ , the ψ fields receive a large mass from the large P field value and are not present in the thermal bath. Assuming that it is gauge-singlet, ψ also does not introduce a coupling of P to gauge bosons. So, the effect of ψ is to introduce a modification of the zero-temperature potential. Assuming that the soft mass squared of $\psi \bar{\psi}$ is positive, quantum corrections to the soft mass of P induced by this coupling steepens the zero-temperature potential and can destabilize Q-balls. So, with an $\mathcal{O}(1)$ coupling y_ψ , for $\mu(S) > T$ the non-quadratic part of the potential of S is

$$V \supset \kappa m_S^2 S^2 \ln \frac{S}{\mu} + \alpha_2^2 T^4 \ln \frac{S}{T}, \quad (4.6)$$

where $\kappa \sim 1/(16\pi^2)$. Q-ball solutions exist if V/S^2 is minimized at non-zero S . The above

potential has a minimum at $S^2 \sim \alpha^2 T^4 / (\kappa m_S^2)$. Requiring self-consistency with the condition $\mu(S) > T$, we obtain

$$T > \frac{1}{g_2^2} \left(\frac{\kappa}{1/16\pi^2} \right)^{1/2} N_{\text{DW}} \frac{m_S}{\mu} f_a \quad (\text{Q-balls : } \mu(S) > T). \quad (4.7)$$

The Q-ball solution may also exist in the regime $\mu(S) < T$, for which the non-quadratic part of the potential of S is

$$V \supset \kappa m_S^2 S^2 \ln \frac{S}{\mu} - c_T y^4 S^4, \quad (4.8)$$

where $y = \mu / (f_a N_{\text{DW}})$ is the coupling between P and $H_u H_d$, $c_T \sim 1 / (16\pi^2)$. Note that the thermal trilinear term $-y^3 S^3 T$ is absent since the Higgs field obtains a large thermal mass $\sim gT$ and the IR singularity is removed. The minimum of V/S^2 is at $S^2 \sim \kappa m_S^2 / (c_T y^4)$. For consistency, this should satisfy $yS < T$, so we obtain

$$T > \left(\frac{\kappa}{c_T} \right)^{1/2} N_{\text{DW}} \frac{m_S}{\mu} f_a \quad (\text{Q-balls : } \mu(S) < T). \quad (4.9)$$

Comparing Eq. (4.7) with Eq. (4.9), the latter gives a slightly stronger condition, so Q-balls disappear when Eq. (4.9) is violated. Unless $T_R \gg f_a$, the production of $B - L$ asymmetry dominantly occurs after Q-balls disappear, so the estimation of $B - L$ asymmetry is not affected by the production of Q-balls. Given current bounds on f_a and constraints on T_R from BBN, we do not expect $T_R \gg f_a$.

For $n = 2$, the potential of S is flatter than a quadratic one only for $\mu(S) > T$. Therefore, even if Q-balls are formed, once the field value of S inside the Q-balls is such that $\mu(S) < T$, Q-balls should disappear. However, this can occur only at a temperature below T_μ , since the field value of S inside the Q-balls is larger than the average field value. With Q-balls at temperatures below T_μ , the estimation of $B - L$ asymmetry may be affected. We may avoid this by a coupling $W = P\psi\bar{\psi}$ as in $n = 1$. So, for $n = 2$, when the condition in Eq. (4.7) is violated, Q-balls disappear.

So, for both $n = 1$ and 2, even if Q-balls form at the early stage of the evolution of the axion rotation, they can disappear by the era when $B - L$ asymmetry is produced by lepto-axiogenesis if there exists a coupling to extra fields $\psi\bar{\psi}$. We stress again that this extra

couplings may not be necessary because the symmetry breaking potential of S may lead to additional effects that destabilize the Q-balls.

We note that the Q-ball formation may lead to production of domain walls. Indeed, Q-ball formation is a result of the growth of fluctuations. As in the parametric resonance during the oscillation of the PQ symmetry breaking field [59, 60], the growth of fluctuations may non-thermally restore the PQ symmetry and produce domain walls. Since $N_{\text{DW}} > 1$ for the DFSZ model, domain walls are stable and will come to dominate the universe. However, we expect that the symmetry restoration would not occur in the two-field model since the PQ symmetry-breaking fields are fixed on the moduli space where the PQ symmetry is broken. In the one-field model, on the other hand, the symmetry restoration might occur. Whether or not the domain wall production actually occurs should be investigated by numerical computation; it is possible that the non-zero angular momentum in field space tends to expel the field from the center and prevent the symmetry restoration.

In summary, it remains to be seen whether or not Q-balls, if formed, are ultimately problematic, and whether they disturb the calculation of the baryon asymmetry. However, coupling the PQ-field to other fields induces quantum corrections to the saxion potential that steepen it and can avert Q-ball production.

5. DISCUSSION

In this work we have explored the possibility that the observed baryon asymmetry arises from the interplay of early-universe dynamics of the axion and the origin of neutrino masses. Under this assumption, we could obtain information on the mass of the saxion, the radial mode of the complex field that contains the axion. In models of gravity mediation, the mass of the saxion would be comparable to the masses of the MSSM particles. So, one can interpret the results as predictions for the masses of the superpartners. We have investigated the DFSZ model in detail including the successful thermalization of the saxion.

For a hierarchical neutrino mass spectrum, the scalar mass may be as low as $\mathcal{O}(10)$ TeV. The observed Higgs boson mass in this case may be explained by moderately large $\tan \beta$. For the scalar mass of $\mathcal{O}(10)$ TeV, the gaugino masses given by the anomaly mediation [67, 68] is below $\mathcal{O}(100)$ GeV, so singlet SUSY-breaking fields must be present to give phenomenologically viable gaugino masses. This generically leads to the Polonyi problem [69], which can

be avoided by a large coupling between the SUSY-breaking fields and the inflaton [70–72] or a coupling between the SUSY-breaking fields and a pseudo-flat direction [73].

Successful thermalization of the rotation typically requires μ different from m_S by an $\mathcal{O}(1)$ factor. For $\mu > m_S$, electroweak symmetry breaking requires the soft masses of the Higgs fields to be also larger than m_S by an $\mathcal{O}(1)$ factor.

If reheat temperatures are somewhat lower than the maximum value considered here, or if the saxion comes to dominate the energy density of the universe at some point in its history, then the scalar mass is required to be larger. Interestingly, after requiring the kinetic misalignment mechanism to explain the observed dark matter abundance, we find the scalar mass is at most 300 TeV. (One can check that the predicted scalar mass is still small enough that the tachyonic instability to create a helical magnetic field is ineffective, so the associated overproduction of the baryon asymmetry recently noted in Ref. [74] is avoided.) The scalar mass of 300 TeV is compatible with the scenario without singlet supersymmetry-breaking fields [68], also known as mini-split SUSY, pure gravity mediation, spread SUSY, etc. In this scenario, the infamous Polonyi problem and the BBN gravitino problem are absent, the SUSY flavor/CP problem mitigated, and the observed Higgs boson mass in this case can be explained with $\tan\beta$ of order unity [75–84]. The dominant contribution to the gaugino mass is given by anomaly mediation [67, 68], and the gauginos may be searched for at the LHC.

As for the axions, we find a preferred region that simultaneously predicts the dark matter and the baryon asymmetry with $f_a \sim 10^9$ GeV, just above the current bound from observations of red giants. This presents a target for experimental searches including the Broadband Reflector Experiment for Axion Detection (BREAD) [85], the Axion Resonant InterAction Detection Experiment (ARIADNE) [86, 87], or other future detectors [88].

Questions regarding the dynamics of the rotating axion field remain. As discussed in Sec. 4.5, Q-balls can form when the saxion potential is flatter than a quadratic one. The spatial distribution of the angular velocity of the axion field after Q-balls form, but prior to their decay, is of importance to accurately estimate the efficiency of axiogenesis scenarios. In Sec. 4.5, we introduced new couplings of the PQ-field to hasten the disappearance of the Q-balls, rendering them irrelevant. However, even in the absence of these additional couplings, we expect Q-balls to eventually decay since the zero-temperature potential does not admit isolated Q-ball solutions. When the decay actually occurs requires additional investigation, perhaps with the help of a lattice computation. Because the requirement of a large initial

field value constrains the potential of the saxion to be nearly quadratic in axiogenesis, the condition for an epoch of Q-ball formation should be satisfied rather generically. This makes answering the fate of axiogenesis in the presence of Q-balls a particularly interesting question.

ACKNOWLEDGEMENTS

The work is supported by the U.S. Department of Energy, Office of Science, under Award number DE-SC0011842 at the University of Minnesota (R.C.) and DE-SC0007859 at the University of Michigan (A.P.).

Appendix A: Computation of chemical potentials

In this appendix, we calculate the chemical potentials for Eq. (3.5), which in turn allow us to compute the $C_i(T)$ of Eq. (3.6) that are necessary to evaluate the baryon asymmetry. To calculate the chemical potentials we apply the principle of detailed balance to scattering processes in equilibrium [47]. This sets the sum of the chemical potentials participating in a given reaction to zero. If a certain scattering process is out of equilibrium, we replace the equilibrium condition with a corresponding conservation law. Solving the resulting system of equations allows for the determination of the chemical potentials.

We will discuss the equilibrium condition for each scattering process and the corresponding conservation laws. In the present case, the scattering processes include Yukawa interactions, electroweak and strong sphaleron processes, gaugino masses, and the μ -term.

1. All interactions in equilibrium

At low temperatures, all Yukawa couplings, sphaleron processes, and mass terms are in thermal equilibrium. Because of the explicit PQ breaking by the QCD anomaly, the rotation is slowly washed out, and it would vanish at the true thermal equilibrium. However, the washout rate is much smaller than the Hubble expansion rate, and the true thermal equilibrium is never reached [10]. Instead, we should consider a quasi-equilibrium state where $\dot{\theta}$ is taken to be constant with its value determined by the potential of the saxion. The quasi-equilibrium can be found by taking the time derivatives of the MSSM particle

number asymmetry in the Boltzmann equations to vanish. The solution to this system of equations depends on the magnitudes of coupling constants. However, because the up-Yukawa coupling is small, it can be set to zero to a good approximation [14]. And while the goal is to find the (quasi)-equilibrium values for the case where the chiral symmetry is completely broken, this procedure, wherein we take the parameter which breaks the chiral asymmetry the least (the up-Yukawa) to vanish, will reproduce the leading contribution to the asymmetry. Then, with this prescription for the up-Yukawa coupling in place, taking the time-derivatives to be zero is equivalent to applying the principle of detailed balance to each scattering process.

The equilibrium conditions for the remaining Yukawa interactions are

$$\mu_{\ell_i} + \mu_{\bar{e}_i} + \mu_{\tilde{H}_d} + \mu_\lambda = 0, \quad (\text{A.1})$$

$$\mu_{Q_2} + \mu_{\bar{u}_2} + \mu_{\tilde{H}_u} + \mu_\lambda = 0, \quad (\text{A.2})$$

$$\mu_{Q_3} + \mu_{\bar{u}_3} + \mu_{\tilde{H}_u} + \mu_\lambda = 0, \quad (\text{A.3})$$

$$\mu_{Q_i} + \mu_{\bar{d}_j} + \mu_{\tilde{H}_d} + \mu_\lambda = 0. \quad (\text{A.4})$$

We have chosen to express equilibrium conditions in terms of the fermionic part of each chiral supermultiplet, and μ_λ is the chemical potential of gauginos. Since the doublet quarks and squarks couple to all gauginos, as long as the gauge interaction is in thermal equilibrium, all gauginos have the same chemical potential. The scalar and fermionic chemical potentials—owing to in equilibrium interactions with gauginos—are related by

$$\mu_\lambda + \mu_\psi - \mu_\phi = 0, \quad (\text{A.5})$$

where ϕ and ψ represent the scalar and fermion part of a chiral supermultiplet, respectively. While the charged lepton and up-quark Yukawa interactions may be taken to be flavor diagonal, in general, there will be off-diagonal components for the down-quarks, see Eq. (A.4). Note that four of the nine equations in Eq. (A.4) are redundant. Among the linearly dependent equilibrium conditions, it is convenient to use those which violate conservation laws with the largest rate. It is that rate which sets the temperature at which the conservation law is broken and the corresponding equilibrium condition is satisfied. We choose the $(i, j) = (1, 1), (1, 2), (2, 2), (2, 3),$ and $(3, 3)$ parts of Eq. (A.4). The equilibrium

conditions for the electroweak and strong sphalerons are

$$\sum_{k=1}^{N_g} (3\mu_{Q_k} + \mu_{\ell_k}) + \mu_{\tilde{H}_u} + \mu_{\tilde{H}_d} + 4\mu_\lambda + c_W \mu_\theta = 0, \quad (\text{A.6})$$

$$\sum_{k=1}^{N_g} (2\mu_{Q_k} + \mu_{\tilde{u}_k} + \mu_{\tilde{d}_k}) + 6\mu_\lambda + c_g \mu_\theta = 0, \quad (\text{A.7})$$

where c_W and c_g are the weak and strong anomaly coefficients of the PQ symmetry. These anomaly coefficients are set to zero in the DFSZ case, but not the KSVZ case. Because ρ_θ is given as $-\dot{\theta}n_\theta$, μ_θ must be $-\dot{\theta}$. Other interactions to consider are chiral-symmetry violation by the gaugino mass and either the standard MSSM μ -term (for KSVZ) or the interaction in Eq. (3.14) (for DFSZ), which give

$$\mu_\lambda = 0, \quad (\text{A.8})$$

$$\mu_{\tilde{H}_u} + \mu_{\tilde{H}_d} + \frac{n}{N_{\text{DW}}} \mu_\theta = 0. \quad (\text{A.9})$$

Setting $n = 0$ in Eq. (A.9) corresponds to taking the standard MSSM μ -term for KSVZ, while taking $n \neq 0$ corresponds to the DFSZ case.

In addition to the above detailed balance relations, we must also impose the conservation laws to determine the asymmetry. With all interactions in thermal equilibrium, the only conservation laws are those of weak hypercharge, $Y = 0$, and $B/3 - L_i$ for each generation i . $B/3 - L_i$ is violated by the superpotential in Eq. (3.1), but this interaction is never close to equilibrium, and it is therefore a small perturbation that may be neglected for the computation of chemical potentials. For $\mu_i, m_i \ll T$, the net fermion and boson densities are given by $n_\psi - n_{\psi^\dagger} = \frac{g}{6} T^2 \mu_\psi$ and $n_\phi - n_{\bar{\phi}} = \frac{g}{3} T^2 \mu_\phi$, so the hypercharge and $B/3 - L_i$ conservation conditions can be expressed in terms of chemical potentials as

$$\sum_{k=1}^{N_g} (\mu_{Q_k} - \mu_{\ell_k} - 2\mu_{\tilde{u}_k} + \mu_{\tilde{d}_k} + \mu_{\tilde{e}_k}) + \mu_{\tilde{H}_u} - \mu_{\tilde{H}_d} = 0, \quad (\text{A.10})$$

$$\sum_{k=1}^{N_g} (2\mu_{Q_k} - \mu_{\tilde{u}_k} - \mu_{\tilde{d}_k}) - 6\mu_{\ell_i} + 3\mu_{\tilde{e}_i} - 2\mu_\lambda = 0. \quad (\text{A.11})$$

2. Out of equilibrium Yukawa interactions

The conservation law that is broken at the lowest temperature is \bar{e}_1 number conservation. This is finally broken when the scattering rate involving the electron Yukawa coupling with rate $\alpha_2 y_e^2 T$ overtakes the Hubble expansion rate. When \bar{e}_1 number is conserved, Eq. (A.1) for $i = 1$ should be replaced by

$$\mu_{\bar{e}_1} = 0. \quad (\text{A.12})$$

This will result in a solution to the chemical potentials for leptons that depends on the generation. The conservation law that persists to the next lowest temperature is $\bar{u}_1 - \bar{d}_1$ number, which is broken by the down-Yukawa interaction with a rate $\alpha_3 |Y_{11}^d|^2 T$. When $\bar{u}_1 - \bar{d}_1$ number is conserved, the $(i, j) = (1, 1)$ component of Eq. (A.4) should be replaced by

$$\mu_{\bar{u}_1} - \mu_{\bar{d}_1} = 0. \quad (\text{A.13})$$

The last symmetry we consider is $3B_1 - B$, which is broken by off-diagonal down-type Yukawa interactions of the first generation with the second and third generations. Because of the large charm and top Yukawa couplings, we take a quark basis where the down-type Yukawa matrix $Y^d = V_{\text{CKM}} \text{diag}(y_d, y_s, y_b)$ and the up-type Yukawa is diagonal. In this basis, the dominant contributions to $3B_1 - B$ breaking are from the interactions of Q_1 with d_2 and d_3 , so the rate of symmetry breaking is $\alpha_3 (|Y_{12}^d|^2 + |Y_{13}^d|^2) T$. When $3B_1 - B$ is conserved, the $(i, j) = (1, 2)$ component of Eq. (A.4) should be replaced by

$$2(2\mu_{Q_1} - \mu_{\bar{u}_1} - \mu_{\bar{d}_1}) - (2\mu_{Q_2} - \mu_{\bar{u}_2} - \mu_{\bar{d}_2}) - (2\mu_{Q_3} - \mu_{\bar{u}_3} - \mu_{\bar{d}_3}) = 0. \quad (\text{A.14})$$

Other Yukawa interactions could be out of equilibrium, but this would occur at high enough temperatures that the $B - L$ production by lepto-axiogenesis is subdominant.

The temperatures at which these different conservation laws are broken are shown in Fig. 9. These are functions of $\tan \beta$ because of the dependence of the MSSM Yukawa matrices on $\tan \beta$. Ignoring threshold corrections from integrating out superpartners, $Y^u = Y_{\text{SM}}^u / \sin \beta$, $Y^d = Y_{\text{SM}}^d / \cos \beta$, and $Y^e = Y_{\text{SM}}^e / \cos \beta$. We take the gauge and SM Yukawa couplings defined at a scale of 10 TeV from Ref. [89] and then run them using the 1-loop

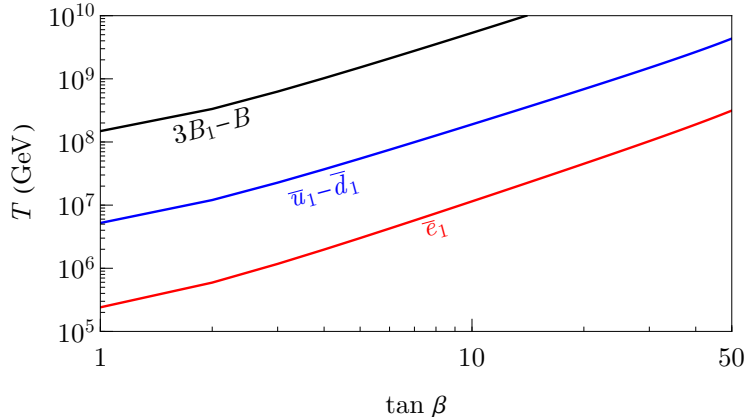


FIG. 9. Temperatures at which conservation laws are broken by Yukawa interactions coming into equilibrium. These temperatures are functions of $\tan \beta$, the ratio of Higgs field vacuum expectation values. The \bar{e}_1 number is broken by the electron-Yukawa interaction, $\bar{u}_1 - \bar{d}_1$ by the down-quark-Yukawa interaction, and $3B_1 - B$ by off-diagonal down-type-quark-Yukawa interactions.

RGEs [90] of the MSSM. In Fig. 9, it is assumed that the Hubble parameter is that of a radiation-dominated universe with $g_* = g_{\text{MSSM}} = 228.75$. A universe with fewer relativistic degrees of freedom would break the symmetries at a higher temperature, while a universe not dominated by radiation would break them at a lower temperature.

Whether or not the high temperatures where these new conservation laws apply are compatible with constraints from supersymmetric relics, see Appendix C, depends on the details of the spectrum.

3. Out of equilibrium gaugino masses and μ -term

At sufficiently high temperatures, scattering due to the gaugino mass or the μ -term may be ineffective.

First, we discuss the gaugino mass. The rate of chiral-symmetry violation by the gaugino mass is $\Gamma \sim m_\lambda^2/T$. Equating this rate with the Hubble expansion rate during a radiation-dominated era, we find this interaction goes out of equilibrium for temperatures above

$$T_\lambda \simeq (m_\lambda^2 M_{\text{Pl}})^{1/3} = 10^8 \text{ GeV} \left(\frac{m_\lambda}{1 \text{ TeV}} \right)^{2/3}. \quad (\text{A.15})$$

Above these temperatures, the chemical potential associated with the gauginos μ_λ will no longer vanish, and it will enter into the equations that result from the Yukawa interactions

	Q	U_1^c	$U_{2,3}^c$	D^c	E^c	L	H_u	H_d
Q_R	1	0	0	0	$\frac{4}{3}$	$-\frac{1}{3}$	1	1
WW'	-1	6	0	0	$-\frac{10}{3}$	$\frac{7}{3}$	1	1

TABLE I. Charge assignments for the superfields for the additional symmetries present at high temperatures. The R -symmetry Q_R is present for large temperatures when the gaugino mass is ineffective. The WW' symmetry (not an R -symmetry) is present when the μ -term is ineffective. The symmetries are chosen to be non-anomalous with respect to $SU(2)$ and $SU(3)$, see text.

and weak and strong sphalerons, see Eqs. (A.1)-(A.4), (A.6), and (A.7). Another chiral symmetry, R -symmetry, is present, and we must impose an additional conservation law in our system of equations.

To find the new conservation law, we must identify the relevant R -symmetry. It should be non-anomalous with respect to $SU(3)$ and $SU(2)$. One set of R -charge assignments for this symmetry for the MSSM superfields is given in Table I. Because this symmetry is an R -symmetry, the charge of the fermions is $Q_\psi = Q_R - 1$. Gauginos have $Q_\lambda = 1$. Contributions to would-be anomalies are $2N_c$ from gauginos, and $Q_R \times N$ from the chiral superfields, where N counts the multiplicity. This allows us to verify that the would-be R - $SU(2)$ - $SU(2)$ anomaly cancels between winos and the leptons ($4 - (4/3)N_g = 0$). The would-be R - $SU(3)$ - $SU(3)$ anomaly cancels between gluinos and the right-handed quarks ($6 + 2N_g(-1) = 0$), where we have combined the contributions from the up-type and down-type quarks. In terms of chemical potentials, the conservation condition for this R -symmetry is

$$12\mu_\lambda + \sum_{k=1}^{N_g} \left[-3(\mu_{\bar{u}_k} + \mu_{\bar{d}_k}) + \frac{1}{3}\mu_{\bar{e}_k} - \frac{8}{3}\mu_{\ell_k} + 12(\mu_{Q_k} + \mu_\lambda) \right. \\ \left. + 4(\mu_{\tilde{H}_u} + \mu_{\tilde{H}_d} + 2\mu_\lambda) + \frac{8}{3}(\mu_{\bar{e}_k} + \mu_\lambda) - \frac{4}{3}(\mu_{\ell_k} + \mu_\lambda) \right] = 0. \quad (\text{A.16})$$

If the axino-gluino-gluon or axino-Higgs-Higgsino coupling were in thermal equilibrium, the axino would contribute μ_λ or $\mu_{\tilde{H}_u} + \mu_{\tilde{H}_d} + \mu_\lambda$ to this expression for the conserved charge. This affects the values of C_i by at most a few percent, so we ignore these possibilities.

In the case of the KSVZ axion, the μ -term is ineffective at temperature higher than Eq. (A.15) with m_λ replaced with μ . We do not expect that there is such a temperature regime in the DFSZ case because the μ -term itself will increase with temperature, keeping it in equilibrium. If such a temperature regime does exist, this results in yet another conserved

symmetry, which can be taken to be a linear combination of the Weinberg-Wilczek Peccei-Quinn (WW) symmetry wherein $Q_{H_u} = Q_{H_d} = 1$, and $Q_Q = Q_L = -1$ and two additional symmetries: $B + L$, and the symmetry under which only the right handed up quark is charged Q_{u1} , ($Q(U^c) = 1$). The resulting charges for a non-anomalous symmetry are given by $WW' = WW + \frac{5}{3}(B + L) + 6Q_{u1} - \frac{5}{3}(B - L)$, where we have added a multiple of the non-anomalous $B - L$ symmetry to give the more convenient charge assignments shown in Table I. In terms of chemical potentials, the WW' conservation condition is

$$18(3\mu_{\bar{u}_1} + 2\mu_\lambda) + 2(3\mu_{H_u} + 3\mu_{H_d} + 4\mu_\lambda) + \sum_{k=1}^{N_g} \left[-6(3\mu_{Q_k} + 2\mu_\lambda) - \frac{10}{3}(3\mu_{\bar{e}_k} + 2\mu_\lambda) + \frac{14}{3}(3\mu_{\ell_k} + 2\mu_\lambda) \right] = 0. \quad (\text{A.17})$$

4. Results for C_i

Solving the relevant system of equations for the μ_i allows determination of C_i , see Eqs. (3.5) and (3.6).

DFSZ: In Table II, we show C_i for the various cases in the DFSZ model. When all Yukawa interactions and the gaugino mass term are in equilibrium, $C_1 = C_2 = C_3 = 0.0459 \frac{n}{N_{\text{DW}}}$, independent of the PMNS mixing angles. When the electron Yukawa is out of equilibrium, the C_i coefficients are slightly different from each other and depend on the PMNS mixing angles. But using PMNS mixing angles $\theta_{12} = 34^\circ$, $\theta_{23} = 48^\circ$, $\theta_{13} = 8.5^\circ$, the C_i coefficients are still all $0.046 \frac{n}{N_{\text{DW}}}$ to two significant digits. Whether the down-Yukawa interaction is out of equilibrium has a more significant impact; in this case the coefficients become $C_1 = 0.0229 \frac{n}{N_{\text{DW}}}$, $C_2 = 0.0203 \frac{n}{N_{\text{DW}}}$, and $C_3 = 0.0182 \frac{n}{N_{\text{DW}}}$, and the resulting asymmetry can be affected by more than a factor of 2. Whether or not the off-diagonal Yukawa interactions with the down quark are in equilibrium has no effect on C_i .

Whether the gaugino mass term is in equilibrium has a small effect. For the cases when the down Yukawa is in equilibrium, the difference is roughly 3%, pushing C_i to $0.0446 \frac{n}{N_{\text{DW}}}$. The effect on the cases where the down is out of equilibrium is similarly small.

KSVZ: In Table III, we show C_i for the various cases in the KSVZ model. The case when the off-diagonal Yukawa interactions with the down quark are out of equilibrium is not shown because it has a small impact on the result. Whether or not these interactions

DFSZ			
m_λ Efficient	All Yukawas Efficient	y_e Inefficient	y_e and y_d Inefficient
C_1	$0.0459 \frac{n}{N_{\text{DW}}}$	$0.0455 \frac{n}{N_{\text{DW}}}$	$0.0229 \frac{n}{N_{\text{DW}}}$
C_2	$0.0459 \frac{n}{N_{\text{DW}}}$	$0.0458 \frac{n}{N_{\text{DW}}}$	$0.0203 \frac{n}{N_{\text{DW}}}$
C_3	$0.0459 \frac{n}{N_{\text{DW}}}$	$0.0461 \frac{n}{N_{\text{DW}}}$	$0.0182 \frac{n}{N_{\text{DW}}}$
m_λ Inefficient	All Yukawas Efficient	y_e Inefficient	y_e and y_d Inefficient
C_1	$0.0446 \frac{n}{N_{\text{DW}}}$	$0.0439 \frac{n}{N_{\text{DW}}}$	$0.0213 \frac{n}{N_{\text{DW}}}$
C_2	$0.0446 \frac{n}{N_{\text{DW}}}$	$0.0444 \frac{n}{N_{\text{DW}}}$	$0.0189 \frac{n}{N_{\text{DW}}}$
C_3	$0.0446 \frac{n}{N_{\text{DW}}}$	$0.0449 \frac{n}{N_{\text{DW}}}$	$0.0170 \frac{n}{N_{\text{DW}}}$

TABLE II. C_i coefficients in the DFSZ model when different reactions are in equilibrium. The first group of rows corresponds to the case when scattering through the gaugino mass is in equilibrium, and the second group corresponds to the case where it is not. The first column of numbers corresponds to the low-temperature case when all Yukawa interactions are in equilibrium. The second corresponds to the case when only interactions via the electron-Yukawa are out of equilibrium, and the third also has down-Yukawa interactions out of equilibrium.

KSVZ			
m_λ and μ Efficient	All Yukawas Efficient	y_e Inefficient	y_e and y_d Inefficient
C_1	$0.0037c_g + 0.0069c_W$	$0.0016c_g + 0.0082c_W$	$-0.0063c_g + 0.0083c_W$
C_2	$0.0037c_g + 0.0069c_W$	$0.0033c_g + 0.0072c_W$	$-0.0055c_g + 0.0074c_W$
C_3	$0.0037c_g + 0.0069c_W$	$0.0047c_g + 0.0064c_W$	$-0.0050c_g + 0.0066c_W$
m_λ Inefficient	All Yukawas Efficient	y_e Inefficient	y_e and y_d Inefficient
C_1	$0.0037c_g + 0.0089c_W$	$0.0016c_g + 0.0098c_W$	$-0.0063c_g + 0.0083c_W$
C_2	$0.0037c_g + 0.0089c_W$	$0.0033c_g + 0.0091c_W$	$-0.0055c_g + 0.0074c_W$
C_3	$0.0037c_g + 0.0089c_W$	$0.0047c_g + 0.0085c_W$	$-0.0050c_g + 0.0067c_W$
m_λ and μ Inefficient	All Yukawas Efficient	y_e Inefficient	y_e and y_d Inefficient
C_1	$-0.0107c_g + 0.0063c_W$	$-0.0126c_g + 0.0072c_W$	$-0.0127c_g + 0.0071c_W$
C_2	$-0.0107c_g + 0.0063c_W$	$-0.0111c_g + 0.0064c_W$	$-0.0112c_g + 0.0064c_W$
C_3	$-0.0107c_g + 0.0063c_W$	$-0.0098c_g + 0.0059c_W$	$-0.0101c_g + 0.0058c_W$

TABLE III. C_i coefficients in the KSVZ model when different reactions are in equilibrium. The first group of rows corresponds to the case when scattering via the gaugino mass and μ -term are in equilibrium. The second group corresponds to the case where the μ -term is in equilibrium but the gaugino mass is not. The third group corresponds to the case where both the gaugino mass and μ -term are out of equilibrium. The first column corresponds to the low-temperature case when all Yukawa interactions are in equilibrium. The second gives results when only the interactions via the electron-Yukawa is out of equilibrium, and the third also has down-Yukawa interactions out of equilibrium. In the standard normalization of the axion-gluon coupling, $c_g = 1$.

are in equilibrium has no effect when scattering via the μ -term is efficient, and an effect only on the level of several percent when the μ -term is inefficient.

Appendix B: Scaling of baryon asymmetry production

To find the baryon asymmetry, it is important to identify which cosmological epoch dominates production. The yield of the $B-L$ asymmetry produced per Hubble time ΔY_{B-L} is given in Eq. (3.7). This quantity is redshift invariant after production if no entropy is subsequently produced. In this case, the dominant epoch can be identified by examining the scaling of $\dot{\theta}$ and the Hubble rate H . On the other hand, if entropy is produced from inflationary reheating/saxion thermalization, it is more convenient to examine

$$\frac{\Delta n_{B-L}}{\rho_{\text{matter}}} \equiv \frac{\dot{n}_{B-L}}{\rho_{\text{matter}} H} = \sum C_i(T) m_{\nu_i}^2 \frac{\dot{\theta} T^5}{\rho_{\text{matter}} H v_{H_u}^4}, \quad (\text{B.1})$$

which is redshift invariant following the production of the asymmetry because both previously produced n_{B-L} and the matter (inflaton or saxion) energy density ρ_{matter} scale as R^{-3} . In Table IV, we summarize how these relevant quantities scale. If the final scaling of $\Delta n_{B-L}/s$ or $\Delta n_{B-L}/\rho_{\text{matter}}$ features an increasing (decreasing) function of R , then the production is IR (UV)-dominated during the corresponding epoch.

For example, if $T_S > T_R$, the table shows that production peaks at T_S during inflationary reheating, labeled as the inflaton non-adiabatic, matter-dominated era $\text{MD}_{\text{NA}}^{\text{inf}}$. This is because $\Delta n_{B-L}/\rho_{\text{inf}}$ is IR-dominated (UV-dominated) before (after) T_S during $\text{MD}_{\text{NA}}^{\text{inf}}$, while $\Delta n_{B-L}/s$ stays UV-dominated in all subsequent eras with $T < T_S$. This result is illustrated in the right panel of Fig. 2.

On the other hand, if $T_S < T_R$, the baryon asymmetry is produced in equal amount in each Hubble time, $\Delta n_{B-L}/s \propto R^0$, during a radiation-dominated era labeled by RD until $T_f = \max(T_S, T_{\text{RM}})$. We first discuss the case without saxion domination, i.e., with early thermalization. At this T_f , the production subsequently becomes UV-dominated because, if $T < T_S$ during radiation domination, $\Delta n_{B-L}/s \propto R^{-3}$ or if $T < T_{\text{RM}}$ (but $T > T_S$) there is a matter-dominated era by the rotation energy density $\text{MD}_{\text{A}}^{\text{rot}}$ and $\Delta n_{B-L}/s \propto R^{-1/2}$ in this era. This (adiabatic) matter-dominated era $\text{MD}_{\text{A}}^{\text{rot}}$ does not result in any entropy production as the energy density ultimately becomes subdominant to radiation due to the era where it scales as kination. This is the case where continuous production leads to the logarithmic enhancement discussed around Eq. (3.9). This case is illustrated in the left panel of Fig. 2.

In the above discussion, we assumed that the saxion energy density was depleted by

Epoch		H	T	Γ_L	ρ_{matter}	$\dot{\theta}$	$\frac{\Delta n_{B-L}}{s}$	$\frac{\Delta n_{B-L}}{\rho_{\text{matter}}}$
$\text{MD}_{\text{NA}}^{\text{inf}}$	$T > T_S$	$R^{-\frac{3}{2}}$	$R^{-\frac{3}{8}}$	$R^{-\frac{9}{8}}$	R^{-3}	R^0	–	$R^{\frac{21}{8}}$
	$T < T_S$					R^{-3}	–	$R^{-\frac{3}{8}}$
RD	$T > T_S$	R^{-2}	R^{-1}	R^{-3}	–	R^0	R^0	–
	$T < T_S$					R^{-3}	R^{-3}	–
$\text{MD}_{\text{NA}}^{\text{osc}}$	$\left\{ \begin{array}{l} \Gamma_{S\tilde{H}\tilde{H}} \\ \Gamma_{SWW} \end{array} \right. T > T_S$	$R^{-\frac{3}{2}}$	$R^{\frac{3}{2}}$	$R^{\frac{9}{2}}$	R^{-3}	R^0	–	R^{12}
	$T > T_S$	$R^{-\frac{3}{2}}$	$R^{-\frac{1}{2}}$	$R^{-\frac{3}{2}}$		R^0	–	R^2
$\text{MD}_{\text{A}}^{\text{rot}}$	$T > T_S$	$R^{-\frac{3}{2}}$	R^{-1}	R^{-3}	–	R^0	$R^{-\frac{1}{2}}$	–
KD	$T < T_S$	R^{-3}	R^{-1}	R^{-3}	–	R^{-3}	R^{-2}	–

TABLE IV. Scaling of quantities relevant for the estimation of the $B - L$ asymmetry. Positive (negative) exponents for R in the final two columns indicate IR (UV)-dominated production. The case that scales as R^0 has equal contributions per Hubble time and so receives a logarithmic enhancement; see text for details. We note that ρ_{matter} represents either ρ_{inf} or ρ_S depending on which one dominates and creates entropy.

thermalization before dominating the total energy density. If instead the saxion comes to dominate and subsequently creates a large amount of entropy from its thermalization, any previously produced baryon asymmetry can be sufficiently diluted so that the production after saxion thermalization dominates. As discussed in Sec. 4.3, during the non-adiabatic era before the end of thermalization, the relevant thermalization processes are saxion-Higgsino and saxion- W scatterings for $n = 1$ and $n = 2$, respectively. Production of n_{B-L} per Hubble time is listed in Table IV for these two cases with the label $\text{MD}_{\text{NA}}^{\text{osc}}$, and one can see that production is IR-dominated for both cases. (We do not show the scaling for $T < T_S$ here; it is never realized in our parameter space.) This verifies that the contribution produced subsequent to thermalization of the saxion dominates over that produced during thermalization. The production after thermalization is again logarithmically enhanced during a radiation-dominated era but now between T_{th} and $\max(T_{\text{RM}}, T_S)$ with T_{RM} given by Eq. (2.13). The results for the saxion domination scenario are presented in Sec. 4.3.

Appendix C: Constraints from supersymmetric relics

In this supersymmetric framework, there are a number of potentially long-lived relics. These relics may provide constraints on the theory. The constraints depend upon the identity

of both the LSP, and if long-lived, the next-to-lightest supersymmetric particle (NLSP). The predictions of Big Bang Nucleosynthesis (BBN) must not be disturbed, and, if stable, the LSP density may not exceed the dark matter density.

Non-gravitino/axino LSP: We first consider the case of the LSP being a superpartner of a Standard Model particle. The constraint on the mass spectrum and/or the reheat temperature from BBN is discussed in [23]. If the gravitino mass $m_{3/2} \sim \text{TeV}$, late gravitino decays will disturb BBN unless the reheat temperature $T_R \lesssim 10^6 \text{ GeV}$. The bound can be relaxed if the LSP is a slepton, but a charged LSP is strongly constrained by searches for heavy hydrogen [91] and a sneutrino LSP is excluded by direct detection experiments.

Because this value for T_R is close to the typical T_{RM} (or even smaller) this means that any logarithmic enhancement, see Eq. (3.9), is necessarily absent, and the prediction for m_S is somewhat modified (increased). If $m_{3/2} \sim 10 \text{ TeV}$, the upper bound is $T_R \lesssim 10^8 \text{ GeV}$.

It is conceivable that $m_{3/2}$ is quite large with mass $\gtrsim 100 \text{ TeV}$, in which case the gravitino decays might be early enough to avoid conflicts with BBN and larger reheat temperatures might be allowed. However, in this case, the scalar mass must be also $\mathcal{O}(100) \text{ TeV}$; otherwise for $m_{3/2} \gg m_S$, the A -term in Eq. (2.5) becomes much larger than m_S , and P is trapped at a minimum with large S . Additionally, in order for the thermal freeze-out abundance of the LSP (say wino or Higgsino) not to be too large, a hierarchy of the type $m_{\text{LSP}} \ll m_S \sim m_{3/2}$ is required. Moreover, even if gravitino decays during BBN are avoided and the LSP thermal abundance is not too large, there is still a danger of non-thermal overproduction of the LSP from gravitino decays. For a gravitino mass of 100 TeV and a LSP mass of a TeV , this constrains the reheat temperature $T_R < 2 \times 10^9 \text{ GeV}$ [23].

The above upper bounds on the reheat temperature could be relaxed if R -parity is violated. In this case, we may assume a slepton LSP, thereby weakening the BBN constraints from gravitino decays, but without conflicting with heavy isotope searches nor direct detection. If there are no sparticles between the gravitino and the slepton(s), the upper bound becomes $T_R < 10^9 (10^{11}) \text{ GeV}$ for $m_{3/2} \sim 1 (10) \text{ TeV}$. For $m_{3/2} > 100 \text{ TeV}$, the LSP overproduction bound disappears and T_R may be much above 10^9 GeV .

Gravitino LSP: To avoid overproduction of a gravitino LSP from thermal processes requires a reheat temperature $T_R < 2 \times 10^9 \text{ GeV} \times (\text{TeV}/m_{3/2})$. In this case a logarithmic enhancement as in Eq. (3.9) can remain. However, avoiding disruption of BBN via decay of the (visible sector) NLSP puts strong constraints on the parameter space if T_R is above

the sparticle masses. The strongest constraints arise [23, 24] when where the NLSP has a large branching ratio to hadrons; constraints are minimized for a sneutrino NLSP. This can be realized by taking the soft mass of $\mathbf{5}$ to be smaller than that of $\mathbf{10}$. Then, the dominant constraint comes from a three-body decay involving a weak boson, whose branching ratio is $\mathcal{O}(10^{-2})$. For the gravitino mass of TeV, the sneutrino NLSP lifetime is around 10^5 s, and from the constraint on the decay into weak gauge bosons derived in [24], we obtain

$$m_{\tilde{\nu}} Y_{\tilde{\nu}} \times \text{Br}(\text{three-body}) < 10^{-14} \Rightarrow m_{\tilde{\nu}} Y_{\tilde{\nu}} < 10^{-12}. \quad (\text{C.1})$$

The freeze-out abundance of a TeV-scale sneutrino would violate this bound. To evade the bound requires $m_{\tilde{\nu}} > 10$ TeV, so that the lifetime of the sneutrino is shorter than 100 s. We may also avoid the bound by taking $m_{\tilde{\nu}} - m_{3/2} < m_Z$. In this case, the decay mode relevant for the BBN constraints becomes a four-body decay with a branching ratio $\sim 10^{-4}$, and the constraint is marginally satisfied.

If the cutoff scale is below the Planck scale, $m_{3/2} \ll m_{\text{NLSP}}$ and the NLSP lifetime may be shorter. For example, with the cutoff scale around the string scale $\sim 10^{17}$ GeV, $m_{3/2} \sim 100$ GeV with $m_{\text{NLSP}} \sim \text{few TeV}$ is possible. The lifetime is then shorter than 100 s, and $m_{\text{NLSP}} Y_{\text{NLSP}} < 10^{-10}$ and 10^{-7} is required for the NLSP with the leading hadronic decay mode and the sneutrino NLSP, respectively. This is satisfied for $m_{\text{NLSP}} = \mathcal{O}(1)$ TeV.

The bound on the mass spectrum may be avoided if R -parity is violated, since the NLSP can decay much before BBN. The gravitino may still be long-lived enough to be dark matter. In this case, R -parity violating couplings could provide an additional source of asymmetry, see [14], but this is small if the couplings are not large.

Axino LSP: The axino should not be the LSP unless R -parity violation is introduced. To see why this is so, recall the saxion is thermalized. Unless this thermalization occurs below the masses of the sparticles, the axino is also thermalized. Unless the axino mass $m_{\tilde{a}}$ is below $\mathcal{O}(100)$ eV, axino dark matter is overproduced. However, even a subdominant component of hot dark matter is constrained, so a stronger bound $m_{\tilde{a}} \lesssim \mathcal{O}(10)$ eV applies [92].

While in some of the parameter space saxion thermalization does occur at $T_{\text{th}} \lesssim m_S$, and it may be possible to avoid thermalization of the axino, it is nevertheless potentially produced in dangerous amounts via freeze-in at higher temperatures. Indeed, unless the $m_{\tilde{a}} \ll \text{TeV}$ —difficult in gravity mediation—the axino is still overproduced. Indeed, the two-

field model gives $m_{\tilde{a}} \simeq m_{3/2}$ because a non-zero vacuum expectation value for X is induced by a supergravity tadpole. In the one-field model, although $m_{\tilde{a}}$ vanishes at tree-level, it is still generated by one-loop quantum corrections. The dominant contribution comes from the Yukawa coupling $yP\psi\bar{\psi}$ and the associated A -term, where this interaction is also responsible for the generation of the logarithmic potential.

The axino LSP can be viable if R -parity violation allows the axino to decay. For example, for $m_{\tilde{a}}$ above the electroweak scale, the axino can decay before BBN via the LH_u operator without giving a too-large neutrino mass. The contribution to the baryon asymmetry from axiogenesis via R -parity violation [14] is subdominant compared to the lepto-axiogenesis contribution. Such a large $m_{\tilde{a}}$ is readily obtained in the two-field model. In the one-field model, generating a loop-induced $m_{\tilde{a}}$ exceeding the electroweak scale places bounds on the supersymmetry-breaking scale. In gravity mediation with a singlet supersymmetry-breaking field, $A \sim m_S$, so $m_{\tilde{a}}$ above the electroweak scale requires $m_S > 10$ TeV. In gravity mediation without singlets, $A \sim 0.01m_S$, so $m_S > 10^6$ GeV would be required.

The upper bound on T_R from BBN is not relaxed in comparison with other cases. Although the gravitino can have dominant decay $\tilde{G} \rightarrow \tilde{a}a$ if it is the NLSP, the axino anyway decays into SM particles, so the BBN constraint still applies.

-
- [1] R. D. Peccei and H. R. Quinn, “CP Conservation in the Presence of Instantons,” *Phys. Rev. Lett.* **38**, 1440–1443 (1977).
 - [2] R. D. Peccei and H. R. Quinn, “Constraints Imposed by CP Conservation in the Presence of Instantons,” *Phys. Rev. D* **16**, 1791–1797 (1977).
 - [3] S. Weinberg, “A New Light Boson?” *Phys. Rev. Lett.* **40**, 223–226 (1978).
 - [4] F. Wilczek, “Problem of Strong P and T Invariance in the Presence of Instantons,” *Phys. Rev. Lett.* **40**, 279–282 (1978).
 - [5] J. Preskill, M. B. Wise, and F. Wilczek, “Cosmology of the Invisible Axion,” *Phys. Lett. B* **120**, 127–132 (1983).
 - [6] L. F. Abbott and P. Sikivie, “A Cosmological Bound on the Invisible Axion,” *Phys. Lett. B* **120**, 133–136 (1983).
 - [7] M. Dine and W. Fischler, “The Not So Harmless Axion,” *Phys. Lett. B* **120**, 137–141 (1983).

- [8] R. T. Co, L. J. Hall, and K. Harigaya, “Axion Kinetic Misalignment Mechanism,” *Phys. Rev. Lett.* **124**, 251802 (2020), [arXiv:1910.14152 \[hep-ph\]](#).
- [9] C. Eröncel, R. Sato, G. Servant, and P. Sørensen, “ALP dark matter from kinetic fragmentation: opening up the parameter window,” *JCAP* **10**, 053 (2022), [arXiv:2206.14259 \[hep-ph\]](#).
- [10] R. T. Co and K. Harigaya, “Axiogenesis,” *Phys. Rev. Lett.* **124**, 111602 (2020), [arXiv:1910.02080 \[hep-ph\]](#).
- [11] R. T. Co, L. J. Hall, and K. Harigaya, “Predictions for Axion Couplings from ALP Cogenesis,” *JHEP* **01**, 172 (2021), [arXiv:2006.04809 \[hep-ph\]](#).
- [12] K. Harigaya and I. R. Wang, “Axiogenesis from $SU(2)_R$ phase transition,” *JHEP* **10**, 022 (2021), [Erratum: *JHEP* 12, 193 (2021)], [arXiv:2107.09679 \[hep-ph\]](#).
- [13] S. Chakraborty, T. H. Jung, and T. Okui, “Composite neutrinos and the QCD axion: Baryogenesis, dark matter, small Dirac neutrino masses, and vanishing neutron electric dipole moment,” *Phys. Rev. D* **105**, 015024 (2022), [arXiv:2108.04293 \[hep-ph\]](#).
- [14] R. T. Co, K. Harigaya, Z. Johnson, and A. Pierce, “R-parity violation axiogenesis,” *JHEP* **11**, 210 (2021), [arXiv:2110.05487 \[hep-ph\]](#).
- [15] R. T. Co, T. Gherghetta, and K. Harigaya, “Axiogenesis with a heavy QCD axion,” *JHEP* **10**, 121 (2022), [arXiv:2206.00678 \[hep-ph\]](#).
- [16] R. T. Co, N. Fernandez, A. Ghalsasi, L. J. Hall, and K. Harigaya, “Lepto-Axiogenesis,” *JHEP* **21**, 017 (2020), [arXiv:2006.05687 \[hep-ph\]](#).
- [17] J. Kawamura and S. Raby, “Lepto-axiogenesis in minimal SUSY KSVZ model,” *JHEP* **04**, 116 (2022), [arXiv:2109.08605 \[hep-ph\]](#).
- [18] A. R. Zhitnitsky, “On Possible Suppression of the Axion Hadron Interactions. (In Russian),” *Sov. J. Nucl. Phys.* **31**, 260 (1980).
- [19] M. Dine, W. Fischler, and M. Srednicki, “A Simple Solution to the Strong CP Problem with a Harmless Axion,” *Phys. Lett. B* **104**, 199–202 (1981).
- [20] J. E. Kim, “Weak Interaction Singlet and Strong CP Invariance,” *Phys. Rev. Lett.* **43**, 103 (1979).
- [21] M. A. Shifman, A. I. Vainshtein, and V. I. Zakharov, “Can Confinement Ensure Natural CP Invariance of Strong Interactions?” *Nucl. Phys. B* **166**, 493–506 (1980).
- [22] S. Weinberg, “Baryon and Lepton Nonconserving Processes,” *Phys. Rev. Lett.* **43**, 1566–1570 (1979).

- [23] M. Kawasaki, K. Kohri, T. Moroi, and A. Yotsuyanagi, “Big-Bang Nucleosynthesis and Gravitino,” *Phys. Rev. D* **78**, 065011 (2008), [arXiv:0804.3745 \[hep-ph\]](#).
- [24] M. Kawasaki, K. Kohri, T. Moroi, and Y. Takaesu, “Revisiting Big-Bang Nucleosynthesis Constraints on Long-Lived Decaying Particles,” *Phys. Rev. D* **97**, 023502 (2018), [arXiv:1709.01211 \[hep-ph\]](#).
- [25] P. Moxhay and K. Yamamoto, “Peccei-Quinn Symmetry Breaking by Radiative Corrections in Supergravity,” *Phys. Lett. B* **151**, 363–366 (1985).
- [26] M. Dine, L. Randall, and S. D. Thomas, “Baryogenesis from flat directions of the supersymmetric standard model,” *Nucl. Phys. B* **458**, 291–326 (1996), [arXiv:hep-ph/9507453](#).
- [27] K. Harigaya, M. Ibe, M. Kawasaki, and T. T. Yanagida, “Dynamics of Peccei-Quinn Breaking Field after Inflation and Axion Isocurvature Perturbations,” *JCAP* **1511**, 003 (2015), [arXiv:1507.00119 \[hep-ph\]](#).
- [28] E. W. Kolb and M. S. Turner, *The Early Universe*, Vol. 69 (1990).
- [29] V. Domcke, K. Harigaya, and K. Mukaida, “Charge transfer between rotating complex scalar fields,” *JHEP* **08**, 234 (2022), [arXiv:2205.00942 \[hep-ph\]](#).
- [30] R. T. Co, D. Dunsy, N. Fernandez, A. Ghalsasi, L. J. Hall, K. Harigaya, and J. Shelton, “Gravitational wave and CMB probes of axion kination,” *JHEP* **09**, 116 (2022), [arXiv:2108.09299 \[hep-ph\]](#).
- [31] Y. Gouttenoire, G. Servant, and P. Simakachorn, “Revealing the Primordial Irreducible Inflationary Gravitational-Wave Background with a Spinning Peccei-Quinn Axion,” (2021), [arXiv:2108.10328 \[hep-ph\]](#).
- [32] Y. Gouttenoire, G. Servant, and P. Simakachorn, “Kination cosmology from scalar fields and gravitational-wave signatures,” (2021), [arXiv:2111.01150 \[hep-ph\]](#).
- [33] A. Dolgov and D. Kirilova, “ON PARTICLE CREATION BY A TIME DEPENDENT SCALAR FIELD,” *Sov. J. Nucl. Phys.* **51**, 172–177 (1990).
- [34] J. H. Traschen and R. H. Brandenberger, “Particle Production During Out-of-equilibrium Phase Transitions,” *Phys. Rev. D* **42**, 2491–2504 (1990).
- [35] L. Kofman, A. D. Linde, and A. A. Starobinsky, “Reheating after inflation,” *Phys. Rev. Lett.* **73**, 3195–3198 (1994), [arXiv:hep-th/9405187](#).
- [36] Y. Shtanov, J. H. Traschen, and R. H. Brandenberger, “Universe reheating after inflation,” *Phys. Rev. D* **51**, 5438–5455 (1995), [arXiv:hep-ph/9407247](#).

- [37] L. Kofman, A. D. Linde, and A. A. Starobinsky, “Towards the theory of reheating after inflation,” *Phys. Rev. D* **56**, 3258–3295 (1997), [arXiv:hep-ph/9704452](#).
- [38] J. Jaeckel, V. M. Mehta, and L. T. Witkowski, “Monodromy Dark Matter,” *JCAP* **01**, 036 (2017), [arXiv:1605.01367 \[hep-ph\]](#).
- [39] J. Berges, A. Chatrchyan, and J. Jaeckel, “Foamy Dark Matter from Monodromies,” *JCAP* **08**, 020 (2019), [arXiv:1903.03116 \[hep-ph\]](#).
- [40] N. Fonseca, E. Morgante, R. Sato, and G. Servant, “Axion fragmentation,” *JHEP* **04**, 010 (2020), [arXiv:1911.08472 \[hep-ph\]](#).
- [41] E. Morgante, W. Ratzinger, R. Sato, and B. A. Stefanek, “Axion fragmentation on the lattice,” *JHEP* **12**, 037 (2021), [arXiv:2109.13823 \[hep-ph\]](#).
- [42] R. T. Co, K. Harigaya, and A. Pierce, “Gravitational waves and dark photon dark matter from axion rotations,” *JHEP* **12**, 099 (2021), [arXiv:2104.02077 \[hep-ph\]](#).
- [43] T. Yanagida, “Horizontal gauge symmetry and masses of neutrinos,” *Proceedings: Workshop on the Unified Theories and the Baryon Number in the Universe: Tsukuba, Japan, February 13-14, 1979*, Conf. Proc. **C7902131**, 95–99 (1979).
- [44] M. Gell-Mann, P. Ramond, and R. Slansky, “Complex Spinors and Unified Theories,” *Supergravity Workshop Stony Brook, New York, September 27-28, 1979*, Conf. Proc. **C790927**, 315–321 (1979), [arXiv:1306.4669 \[hep-th\]](#).
- [45] P. Minkowski, “ $\mu \rightarrow e\gamma$ at a Rate of One Out of 10^9 Muon Decays?” *Phys. Lett.* **67B**, 421–428 (1977).
- [46] R. N. Mohapatra and G. Senjanovic, “Neutrino Mass and Spontaneous Parity Nonconservation,” *Phys. Rev. Lett.* **44**, 912 (1980), [231(1979)].
- [47] J. A. Harvey and M. S. Turner, “Cosmological baryon and lepton number in the presence of electroweak fermion number violation,” *Phys. Rev. D* **42**, 3344–3349 (1990).
- [48] N. Aghanim *et al.* (Planck), “Planck 2018 results. VI. Cosmological parameters,” *Astron. Astrophys.* **641**, A6 (2020), [arXiv:1807.06209 \[astro-ph.CO\]](#).
- [49] J. E. Kim and H. P. Nilles, “The mu Problem and the Strong CP Problem,” *Phys. Lett. B* **138**, 150–154 (1984).
- [50] D. Bodeker, “Moduli decay in the hot early Universe,” *JCAP* **0606**, 027 (2006), [arXiv:hep-ph/0605030 \[hep-ph\]](#).
- [51] M. Laine, “On bulk viscosity and moduli decay,” *Prog. Theor. Phys. Suppl.* **186**, 404–416

- (2010), [arXiv:1007.2590 \[hep-ph\]](#).
- [52] K. Mukaida and K. Nakayama, “Dynamics of oscillating scalar field in thermal environment,” *JCAP* **1301**, 017 (2013), [arXiv:1208.3399 \[hep-ph\]](#).
- [53] F. Capozzi and G. Raffelt, “Axion and neutrino bounds improved with new calibrations of the tip of the red-giant branch using geometric distance determinations,” *Phys. Rev. D* **102**, 083007 (2020), [arXiv:2007.03694 \[astro-ph.SR\]](#).
- [54] O. Straniero, C. Pallanca, E. Dalessandro, I. Dominguez, F. R. Ferraro, M. Giannotti, A. Mirizzi, and L. Piersanti, “The RGB tip of galactic globular clusters and the revision of the axion-electron coupling bound,” *Astron. Astrophys.* **644**, A166 (2020), [arXiv:2010.03833 \[astro-ph.SR\]](#).
- [55] T. Cohen, M. Lisanti, A. Pierce, and T. R. Slatyer, “Wino Dark Matter Under Siege,” *JCAP* **10**, 061 (2013), [arXiv:1307.4082 \[hep-ph\]](#).
- [56] J. Fan and M. Reece, “In Wino Veritas? Indirect Searches Shed Light on Neutralino Dark Matter,” *JHEP* **10**, 124 (2013), [arXiv:1307.4400 \[hep-ph\]](#).
- [57] R. T. Co, E. Gonzalez, and K. Harigaya, “Increasing Temperature toward the Completion of Reheating,” *JCAP* **11**, 038 (2020), [arXiv:2007.04328 \[astro-ph.CO\]](#).
- [58] R. T. Co, L. J. Hall, K. Harigaya, K. A. Olive, and S. Verner, “Axion Kinetic Misalignment and Parametric Resonance from Inflation,” *JCAP* **08**, 036 (2020), [arXiv:2004.00629 \[hep-ph\]](#).
- [59] S. Kasuya, M. Kawasaki, and T. Yanagida, “Cosmological axion problem in chaotic inflationary universe,” *Phys. Lett. B* **409**, 94–100 (1997), [arXiv:hep-ph/9608405](#).
- [60] S. Kasuya and M. Kawasaki, “Topological defects formation after inflation on lattice simulation,” *Phys. Rev. D* **58**, 083516 (1998), [arXiv:hep-ph/9804429](#).
- [61] P. Sikivie, “Of Axions, Domain Walls and the Early Universe,” *Phys. Rev. Lett.* **48**, 1156–1159 (1982).
- [62] S. R. Coleman, “Q-balls,” *Nucl. Phys. B* **262**, 263 (1985), [Addendum: *Nucl.Phys.B* 269, 744 (1986)].
- [63] A. Kusenko, “Solitons in the supersymmetric extensions of the standard model,” *Phys. Lett. B* **405**, 108 (1997), [arXiv:hep-ph/9704273](#).
- [64] A. Kusenko and M. E. Shaposhnikov, “Supersymmetric Q balls as dark matter,” *Phys. Lett. B* **418**, 46–54 (1998), [arXiv:hep-ph/9709492](#).
- [65] S. Kasuya and M. Kawasaki, “Q ball formation through Affleck-Dine mechanism,” *Phys. Rev.*

- D **61**, 041301 (2000), [arXiv:hep-ph/9909509](#).
- [66] M. Dine and A. Kusenko, “The Origin of the matter - antimatter asymmetry,” *Rev. Mod. Phys.* **76**, 1 (2003), [arXiv:hep-ph/0303065](#).
- [67] L. Randall and R. Sundrum, “Out of this world supersymmetry breaking,” *Nucl. Phys. B* **557**, 79–118 (1999), [arXiv:hep-th/9810155](#).
- [68] G. F. Giudice, M. A. Luty, H. Murayama, and R. Rattazzi, “Gaugino mass without singlets,” *JHEP* **12**, 027 (1998), [arXiv:hep-ph/9810442](#).
- [69] G. D. Coughlan, W. Fischler, E. W. Kolb, S. Raby, and G. G. Ross, “Cosmological Problems for the Polonyi Potential,” *Phys. Lett. B* **131**, 59–64 (1983).
- [70] A. D. Linde, “Relaxing the cosmological moduli problem,” *Phys. Rev. D* **53**, R4129–R4132 (1996), [arXiv:hep-th/9601083](#).
- [71] F. Takahashi and T. T. Yanagida, “Why have supersymmetric particles not been observed?” *Phys. Lett. B* **698**, 408–410 (2011), [arXiv:1101.0867 \[hep-ph\]](#).
- [72] K. Nakayama, F. Takahashi, and T. T. Yanagida, “Gravity mediation without a Polonyi problem,” *Phys. Lett. B* **714**, 256–261 (2012), [arXiv:1203.2085 \[hep-ph\]](#).
- [73] K. Harigaya, M. Ibe, K. Schmitz, and T. T. Yanagida, “A Simple Solution to the Polonyi Problem in Gravity Mediation,” *Phys. Lett. B* **721**, 86–89 (2013), [arXiv:1301.3685 \[hep-ph\]](#).
- [74] V. Domcke, K. Kamada, K. Mukaida, K. Schmitz, and M. Yamada, “A new constraint on primordial lepton flavour asymmetries,” (2022), [arXiv:2208.03237 \[hep-ph\]](#).
- [75] J. D. Wells, “Implications of supersymmetry breaking with a little hierarchy between gauginos and scalars,” in *11th International Conference on Supersymmetry and the Unification of Fundamental Interactions* (2003) [arXiv:hep-ph/0306127](#).
- [76] N. Arkani-Hamed and S. Dimopoulos, “Supersymmetric unification without low energy supersymmetry and signatures for fine-tuning at the LHC,” *JHEP* **06**, 073 (2005), [arXiv:hep-th/0405159](#).
- [77] G. F. Giudice and A. Romanino, “Split supersymmetry,” *Nucl. Phys. B* **699**, 65–89 (2004), [Erratum: *Nucl.Phys.B* 706, 487–487 (2005)], [arXiv:hep-ph/0406088](#).
- [78] J. D. Wells, “PeV-scale supersymmetry,” *Phys. Rev. D* **71**, 015013 (2005), [arXiv:hep-ph/0411041](#).
- [79] M. Ibe, T. Moroi, and T. T. Yanagida, “Possible Signals of Wino LSP at the Large Hadron Collider,” *Phys. Lett. B* **644**, 355–360 (2007), [arXiv:hep-ph/0610277](#).

- [80] B. S. Acharya, K. Bobkov, G. L. Kane, P. Kumar, and J. Shao, “Explaining the Electroweak Scale and Stabilizing Moduli in M Theory,” *Phys. Rev. D* **76**, 126010 (2007), [arXiv:hep-th/0701034](#).
- [81] L. J. Hall and Y. Nomura, “Spread Supersymmetry,” *JHEP* **01**, 082 (2012), [arXiv:1111.4519 \[hep-ph\]](#).
- [82] M. Ibe and T. T. Yanagida, “The Lightest Higgs Boson Mass in Pure Gravity Mediation Model,” *Phys. Lett. B* **709**, 374–380 (2012), [arXiv:1112.2462 \[hep-ph\]](#).
- [83] A. Arvanitaki, N. Craig, S. Dimopoulos, and G. Villadoro, “Mini-Split,” *JHEP* **02**, 126 (2013), [arXiv:1210.0555 \[hep-ph\]](#).
- [84] N. Arkani-Hamed, A. Gupta, D. E. Kaplan, N. Weiner, and T. Zorawski, “Simply Unnatural Supersymmetry,” (2012), [arXiv:1212.6971 \[hep-ph\]](#).
- [85] J. Liu *et al.* (BREAD), “Broadband Solenoidal Haloscope for Terahertz Axion Detection,” *Phys. Rev. Lett.* **128**, 131801 (2022), [arXiv:2111.12103 \[physics.ins-det\]](#).
- [86] A. Arvanitaki and A. A. Geraci, “Detecting high-frequency gravitational waves with optically-levitated sensors,” *Phys. Rev. Lett.* **110**, 071105 (2013), [arXiv:1207.5320 \[gr-qc\]](#).
- [87] A. A. Geraci *et al.* (ARIADNE), “Progress on the ARIADNE axion experiment,” *Springer Proc. Phys.* **211**, 151–161 (2018), [arXiv:1710.05413 \[astro-ph.IM\]](#).
- [88] C. B. Adams *et al.*, “Axion Dark Matter,” in *2022 Snowmass Summer Study* (2022) [arXiv:2203.14923 \[hep-ex\]](#).
- [89] S. Antusch and V. Maurer, “Running quark and lepton parameters at various scales,” *JHEP* **11**, 115 (2013), [arXiv:1306.6879 \[hep-ph\]](#).
- [90] S. P. Martin and M. T. Vaughn, “Two loop renormalization group equations for soft supersymmetry breaking couplings,” *Phys. Rev. D* **50**, 2282 (1994), [Erratum: *Phys.Rev.D* 78, 039903 (2008)], [arXiv:hep-ph/9311340](#).
- [91] S. Burdin, M. Fairbairn, P. Mermoud, D. Milstead, J. Pinfold, T. Sloan, and W. Taylor, “Non-collider searches for stable massive particles,” *Phys. Rept.* **582**, 1–52 (2015), [arXiv:1410.1374 \[hep-ph\]](#).
- [92] W. L. Xu, J. B. Muñoz, and C. Dvorkin, “Cosmological constraints on light but massive relics,” *Phys. Rev. D* **105**, 095029 (2022), [arXiv:2107.09664 \[astro-ph.CO\]](#).